



Variability in clear-sky longwave radiative cooling of the atmosphere

Richard P. Allan¹

Received 16 March 2006; revised 9 June 2006; accepted 2 August 2006; published 18 November 2006.

[1] The longwave radiative cooling of the clear-sky atmosphere (Q_{LWc}) is a crucial component of the global hydrological cycle and is composed of the clear-sky outgoing longwave radiation to space (OLRc) and the net downward minus upward clear-sky longwave radiation to the surface (SNLc). Estimates of Q_{LWc} from reanalyses and observations are presented for the period 1979–2004. Compared to other reanalyses data sets, the European Centre for Medium-range Weather Forecasts 40-year reanalysis (ERA40) produces the largest Q_{LWc} over the tropical oceans (217 W m^{-2}), explained by the least negative SNLc. On the basis of comparisons with data derived from satellite measurements, ERA40 provides the most realistic Q_{LWc} climatology over the tropical oceans but exhibits a spurious interannual variability for column integrated water vapor (CWV) and SNLc. Interannual monthly anomalies of Q_{LWc} are broadly consistent between data sets with large increases during the warm El Niño events. Since relative humidity (RH) errors applying throughout the troposphere result in compensating effects on the cooling to space and to the surface, they exert only a marginal effect on Q_{LWc} . An observed increase in CWV with surface temperature of $3 \text{ kg m}^{-2} \text{ K}^{-1}$ over the tropical oceans is important in explaining a positive relationship between Q_{LWc} and surface temperature, in particular over ascending regimes; over tropical ocean descending regions this relationship ranges from 3.6 to $4.6 \pm 0.4 \text{ W m}^{-2} \text{ K}^{-1}$ for the data sets considered, consistent with idealized sensitivity tests in which tropospheric warming is applied and RH is held constant and implying an increase in precipitation with warming.

Citation: Allan, R. P. (2006), Variability in clear-sky longwave radiative cooling of the atmosphere, *J. Geophys. Res.*, *111*, D22105, doi:10.1029/2006JD007304.

1. Introduction

[2] Globally, the atmosphere experiences a net radiation deficit of approximately 100 W m^{-2} resulting from the dominance of longwave radiative cooling over the absorption of shortwave radiation [e.g., *Kiehl and Trenberth, 1997*]. This cooling is balanced by a transfer of energy from the surface, the majority of which is delivered by surface evaporative cooling and subsequent net latent heat release in the atmosphere once water is removed via precipitation. This radiative-convective balance, or equilibrium [e.g., *Manabe and Wetherald, 1967*], is crucial for the atmospheric hydrological cycle which influences the distribution and supply of fresh water, vital for ecosystems and water resource and risk management.

[3] Since the atmospheric hydrological cycle is inextricably linked to the atmospheric radiative cooling, it is valuable to monitor and quantify this parameter. Clouds represent an important component of this coupling both in relation to latent energy release and also the radiative

heating and cooling of the atmosphere. Using data from the International Satellite Cloud Climatology Project, *Sohn [1999]* found that atmospheric longwave radiative cooling is reduced over convective regions by high-altitude cirrus cloud and is enhanced by low-altitude clouds over dry descending branches of the tropical circulation but that the magnitude of cloud longwave radiative effect is typically only 20% of the total longwave radiative cooling. Further, consistency amongst observational data sets measuring decadal fluctuations in global or tropical cloudiness has yet to be established [*Wielicki et al., 2002; Trenberth, 2002; Zhang et al., 2004; Norris, 2005; Wylie et al., 2005*]. Considering the uncertainty associated with variations in cloudiness and because the majority of radiative cooling is explained by the clear-sky atmosphere, the present study aims to examine in detail the longwave radiative cooling of the clear-sky atmosphere (Q_{LWc}).

[4] A key parameter in determining atmospheric radiative cooling is water vapor [e.g., *Stephens et al., 1994*]. Increased tropospheric humidity reduces radiative cooling to space [e.g., *Spencer and Braswell, 1997; Harries, 1997*]. However, higher water vapor concentration enhances the longwave radiative cooling of the atmosphere to the surface [e.g., *Ramanathan, 1981; Lubin, 1994*]; this is only partially offset by increased shortwave radiative absorption [e.g., *Mitchell*

¹Environmental Systems Science Centre, University of Reading, Reading, UK.

et al., 1987]. Near to the surface, large portions of the longwave spectrum are saturated because of water vapor absorption, more especially in the moist tropics. Therefore the surface may only cool significantly by longwave radiative emission in the more transparent (or window) regions of the spectrum. Here, the lower tropospheric radiative cooling is dominated by water vapor continuum absorption [e.g., *Kilsby et al.*, 1992] which rises rapidly with water vapor concentration. Since these moist, near-surface layers contribute the most to column integrated water vapor (*CWV*), this explains the strong dependence of Q_{LWc} on *CWV* over the tropical oceans [*Stephens et al.*, 1994].

[5] The theoretical relationships between surface temperature (T_s), *CWV* and Q_{LWc} have important implications for climate change. The water vapor holding capacity of the atmosphere approximately scales exponentially with temperature because of the Clausius Clapeyron equations, explaining an observed increase of $\sim 7\% \text{ K}^{-1}$ in the tropics [*Wentz and Schabel*, 2000; *Trenberth et al.*, 2005]. Increases in precipitation with temperature are thought to be about half this value [e.g., *Allen and Ingram*, 2002] because it is constrained by the atmospheric radiative cooling which is limited by saturation of the water vapor absorption bands; this suggests profound changes in the atmospheric hydrological cycle [e.g., *Soden*, 2000; *Allen and Ingram*, 2002; *Hartmann and Larson*, 2002; *Trenberth et al.*, 2003; *Bosilovich et al.*, 2005]. Thus a motivation for the present study is the possible impact of interrelationships between T_s , *CWV* and Q_{LWc} on precipitation.

[6] Although observations of radiative cooling to space from satellite instruments [e.g., *Wielicki et al.*, 2002] provide near-global coverage, temporal sampling is often poor. Conversely, measurements of radiative fluxes at the surface [e.g., *Wild et al.*, 2001; *Philipona et al.*, 2005] are available at high temporal resolution (e.g., minutes) but offer a spatially sparse network. Consequently, it is common to estimate global surface fluxes using empirical formulae [e.g., *Gupta*, 1989] or by supplying atmospheric profiles as input to radiative transfer schemes [e.g., *Slingo et al.*, 2000; *Zhang et al.*, 2004]. Another profitable method is to use atmospheric reanalyses. These use the available network of bias corrected observations via a self consistent data assimilation system and general circulation model, to estimate the atmospheric state required to compute radiative fluxes. Because the changing quality and availability of the observations can cause spurious variations in the reanalysis products, it is necessary to intercompare such data sets with independent observations such that the quality and consistency between products may be estimated [e.g., *Trenberth et al.*, 2005].

[7] The aim of the present study is to provide such an intercomparison of data sets, including from reanalyses, that estimate the clear-sky longwave radiative cooling of the atmosphere, Q_{LWc} . Previous research has concentrated on the regional and seasonal variation of Q_{LWc} derived from satellite data or reanalyses [e.g., *Stephens et al.*, 1994; *Chéruy and Chevallier*, 2000]. Here, we extend these studies by also quantifying the interannual and decadal changes in Q_{LWc} and its determinant variables. *Soden* [2000] provided an analysis of interannual changes in all-sky radiative fluxes at the top of atmosphere and the surface and related variables. In a similar manner, but analyzing clear-sky radiative cooling, the present study

considers the extended time period, 1979–2004; this spans multiple El Niño Southern Oscillation (ENSO) events and includes satellite measurements from a variety of instruments described in section 2.

2. Data and Method

[8] A combination of reanalysis and observationally based data sets that represent clear-sky atmospheric longwave radiative cooling are now described.

2.1. Reanalysis Data

[9] Atmospheric data assimilation combines a general circulation model with an array of high-quality observations that vary in spatial and temporal coverage, to produce an estimate of the three dimensional state of the atmosphere (or analysis). Reanalyses use self-consistent assimilation systems (unchanging with time, unlike operational analyses) that can provide valuable information on the atmosphere, stored on model grids.

[10] In the present study, monthly mean reanalysis data is extracted from the National Centers for Environmental Prediction/National Center for Atmospheric research reanalysis (NCEP [*Kalnay et al.*, 1996]) for the period 1979–2004 on a 1.875° longitude and 1.9° latitude grid. Surface emissivity (ϵ_s) is fixed at unity and greenhouse gases are held fixed.

[11] Monthly mean data on a $2.5 \times 2.5^\circ$ grid were taken from the European Centre for Medium-range Weather Forecast 40-year reanalysis product (ERA40 [*Uppala et al.*, 2005]) over the period 1979–2001. Radiatively active greenhouse gases were updated annually. Outside the window region of the longwave spectrum and for open oceans across the whole spectrum, $\epsilon_s = 0.99$; in the window region, surface emissivity depends on scene type and water content, ranging from 0.93 to 0.98. Climatological surface albedo, vegetation, ozone and aerosol fields were used in the radiative calculations.

[12] Release 2 of the NASA Surface Radiation Budget longwave product [*Stackhouse et al.*, 1999] uses satellite radiances, data assimilation and radiative transfer models to calculate the surface and top of atmosphere radiative fluxes on a $1 \times 1^\circ$ grid over the period 1983–1994. Clear-sky longwave radiation data at the surface and top of atmosphere are employed in the present study. These fields depend primarily on the Goddard GOES-I reanalysis product [*Bloom et al.*, 2005]. Surface emissivity is prescribed on the basis of an observed global climatology. Greenhouse gases are held fixed and aerosol is not included in the longwave radiative transfer calculations.

2.2. Satellite Data

[13] Microwave radiometers on board polar orbiting operational satellites have provided estimates of column integrated water vapor (*CWV*) over the oceans since 1979. Data from the Scanning Multichannel Microwave Radiometer (SMMR [*Wentz and Francis*, 1992]) for 1979–1984 (1° resolution) and the Special Sensor Microwave Imager (SSM/I, version 5 [*Wentz*, 1997]) for 1987–2004 (0.25° resolution) are used in the present study. The SSM/I data are regarded as realistic in terms of means, variability and trends [*Trenberth et al.*, 2005] and are therefore an important tool in evaluating models and reanalyses.

[14] Monthly mean clear-sky outgoing longwave radiation (OLRc) data were taken from the Earth Radiation Budget Satellite (ERBS) for the period 1985–1989, the Scanner for Radiation Budget (ScaRaB) for 1994/1995 and the Clouds and the Earth’s Radiant Energy System (CERES) on the TRMM satellite for 1998 (Version ES4_TRMM-PFM_EDITION2_015013) and on the TERRA satellite from 2000 to 2004 (Version ES4_Terra-FM1_Edition2_024026). For details see *Wielicki et al.* [2002, and references therein].

[15] Monthly mean surface temperature (T_s) on a $1 \times 1^\circ$ grid over the ocean were taken from the Hadley Centre global sea-Ice and Sea Surface Temperature (HadISST) data set [Rayner et al., 2003].

2.3. Empirical Estimation of Clear-Sky Surface Net Longwave Radiation

[16] The clear-sky surface net longwave radiation (SNLc) is defined here as,

$$SNLc = \epsilon_s(SDLc - \sigma T_s^4), \quad (1)$$

where SDLc is the clear-sky surface downwelling longwave radiation, σT_s^4 is the surface upwelling emission, ϵ_s is the surface broadband longwave emissivity and σ is the Stefan-Boltzmann constant. Providing that surface temperature is known to good accuracy, the surface longwave emission can be well simulated. Downward longwave fluxes at the surface are determined primarily by the lower levels of the atmosphere [e.g., Gupta, 1989] which are difficult to estimate using space-based instruments. While SDLc is observable using ground based instruments [e.g., Philipona et al., 2005], measurements are sparse compared to satellite coverage. Reanalysis data can provide realistic estimates of SDLc provided that the atmospheric profiles and the radiative transfer codes are accurate. Despite some promising results with recent reanalysis products in terms of climatologies, there remain spurious decadal variations [e.g., Allan et al., 2004] that are likely to influence the variability in clear-sky longwave radiative cooling. An alternative approach is to estimate SDLc using empirical techniques. For example, Gupta [1989] used satellite estimates of CWV and lower tropospheric temperatures to indirectly estimate clear-sky surface longwave radiation. In the present study we adopt a comparable approach, described below.

[17] The longwave radiative flux at the surface is dominated by water vapor emission. Over the moist, tropical oceans, much of the longwave electromagnetic spectrum is saturated with respect to water vapor; here downward emission approximates to a black body and is determined mainly by the emission temperature of the near surface layer (T_0). Since T_0 is generally close to the temperature of the surface, the upward and downward longwave radiative flux are similar in this portion of the spectrum. In the atmospheric window region of the spectrum (8–14 μm) water vapor continuum emission dominates and this scales with CWV. Thus the SDLc is strongly determined by T_0 and CWV and it is these parameters that are most important for accurate estimation of SDLc and therefore SNLc.

[18] Assuming that T_0 is well coupled to T_s on a decadal timescale, the most important parameter in terms of SDLc

variability is the CWV. Reanalyses have been shown to exhibit spurious variability in CWV [Allan et al., 2004] and the most accurate depiction of CWV variability over the ocean is provided by SSM/I data [Trenberth et al., 2005]. In the present study we use the Prata [1996] empirical relationship to determine SDLc using microwave measurements of CWV over the ocean from the SMMR and SSM/I series of satellites, and estimating T_0 using HadISST and climatological data. The Prata formula is based on radiative transfer theory and calibrated using ground based radiometric observations. SDLc is calculated as,

$$SDLc = \left[1 - \left(1 + \frac{CWV}{k} \right) \exp \left\{ - \left(1.2 + \frac{3CWV}{k} \right)^{\frac{1}{3}} \right\} \right] \sigma T_0^4, \quad (2)$$

where $k = 10 \text{ kg m}^{-2}$. To estimate T_0 , monthly climatological estimates of sea surface minus near-surface temperature (T_{diff}) from da Silva et al. [1994] are subtracted from HadISST T_s at each ocean grid point:

$$T_0 = T_s - T_{diff}. \quad (3)$$

The empirical estimate of SNLc is calculated using equation (1) and setting ϵ_s to unity. This is a reasonable approximation over the ocean, where the empirical estimate is applied. The calculation of SNLc over desert regions is however sensitive to the prescription of ϵ_s and therefore of importance to the reanalysis data sets considered.

[19] The formula in equation (2) is applied using monthly mean HadISST and SMMR-SSM/I data. Using SSM/I data from July 2004, it was found that applying monthly rather than instantaneous SSM/I data for July 2004 contributes to a positive SDLc bias of about 1 W m^{-2} . This bias is removed on calculating anomalies. Prata [1996] estimated a bias of 0.8 W m^{-2} and a root mean squared difference of 6.1 W m^{-2} relative to calculations with climatological radiosonde profiles and a radiative transfer scheme. These uncertainties can be considered an upper limit since the Prata formula used surface variables to estimate CWV whereas in the present study CWV is prescribed using satellite observations. The resulting empirical estimates of SDLc over the ocean provide a valuable independent comparison with the reanalysis and SRB data.

2.4. Calculation of Clear-Sky Atmospheric Longwave Radiative Cooling, Q_{LWc}

[20] Estimates of the clear-sky atmospheric longwave radiative cooling (Q_{LWc}) and determinant variables were calculated over the period 1979–2004 from ERA40, NCEP, SRB and estimated from the suit of available observations (OBS). Note that OBS includes the empirical estimate of SNLc; although this is not an observation, we use OBS for convenience. Monthly mean Q_{LWc} was calculated as the sum of clear-sky outgoing longwave radiation to space (OLRc) and clear-sky surface net longwave radiation (SNLc) as,

$$Q_{LWc} = OLRc + SNLc. \quad (4)$$

Outgoing fluxes from the atmosphere are thus defined as positive. Since the surface longwave emission is generally

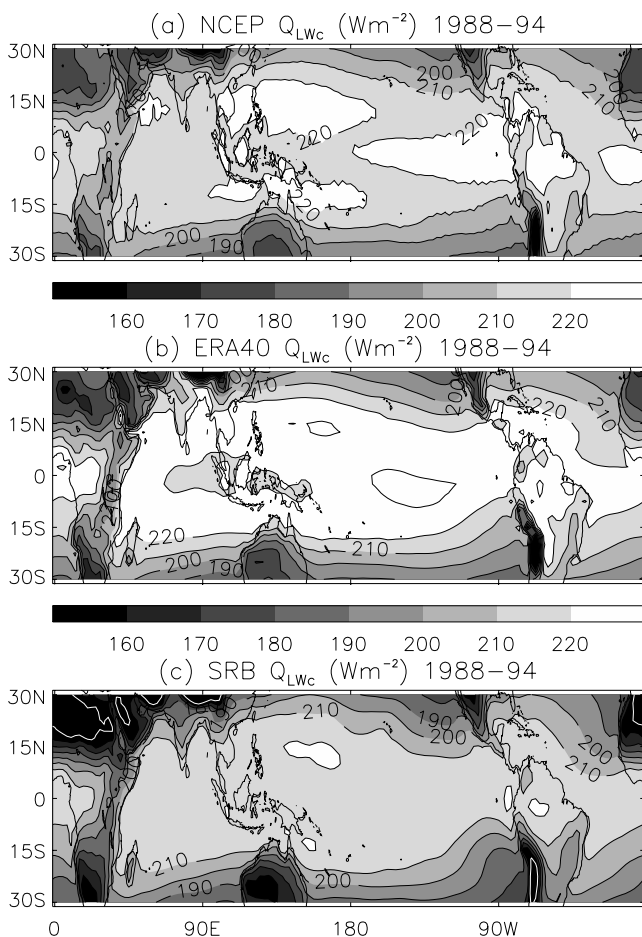


Figure 1. Mean clear-sky longwave radiative cooling of the atmosphere (Q_{LWc}) for (a) NCEP, (b) ERA40 and (c) SRB over the period 1988–1994. Additional contours are placed at 150 W m^{-2} (white) and 230 W m^{-2} (black).

greater than the downward emission from the atmosphere, SNLc is predominantly negative, representing a net heating of the atmosphere. For ERA40 and SRB, both OLRc and SNLc are provided. For NCEP, SNLc was calculated using equation (1) and setting $\epsilon_s = 1.0$, consistent with the value used by the NCEP reanalysis. For OBS, the SNLc is estimated over the oceans using equations (1)–(3) and prescribing $\epsilon_s = 1.0$, as described in section 2.3.

3. Climatology

[21] The multiannual mean (1988–1994) tropical climatology of clear-sky longwave radiative cooling from the atmosphere is presented in Figure 1 for the NCEP, ERA40 and SRB data sets. All data sets are mapped onto a $2.5 \times 2.5^\circ$ grid. The maximum values of Q_{LWc} (cooling) occur over the tropical oceans although slightly lower values are to be found over the marine stratocumulus regions (Peruvian, Californian, Namibian and Canarian), as previously noted by Chéruy and Chevallier [2000]. The lowest values are found over dry desert land regions such as the Sahara and Australia. Despite the general agreement, the magnitude of Q_{LWc} varies between data sets. ERA40 exhibits the strongest oceanic cooling with values above 230 W m^{-2} over the central Pacific (black contour). The ERA40 mean

Q_{LWc} over the tropical oceans is about 4 W m^{-2} larger than NCEP and 9 W m^{-2} greater than SRB (Table 1). The SRB data set produces the smallest atmospheric cooling globally and in particular over the Sahara where $Q_{LWc} < 150 \text{ W m}^{-2}$ (white contour in Figure 1c). Comparing the standard deviations in Table 1, spatial variability is largest for the global domain for Q_{LWc} and OLRc, being of order 15 to 20% of the mean values whereas the SNLc standard deviation is of this proportion of the mean SNLc for all domains considered. It is apparent that the NCEP data in general exhibits a smaller spatial variability than the other data sets.

[22] To understand the reasons for the differences in Q_{LWc} it is informative to partition the cooling between top of atmosphere (Figure 2) and surface contributions (Figure 3). The mean OLRc is largest over the dry, descending portions of the Hadley circulation, in particular the Sahara and the southeast Pacific (Figure 2). Minimum values of clear-sky OLR are found over the moist regions of the intertropical convergence zone but also more particularly for the cold, mountainous regions (Andes and Himalayas). The distributions of OLRc for ERA40 and SRB are in reasonable agreement while the NCEP data produces larger values over the desert regions (Australia and Sahara) and smaller values over the tropical warm pool. Globally, NCEP produces clear-sky OLR 3.5 W m^{-2} larger than ERA40 and 5.5 W m^{-2} greater than SRB (Table 1).

[23] Since satellite clear-sky data only samples the anomalous cloud-free times, which are drier and therefore produce lower thermal emission, these data sets are not considered in the OLRc comparisons. However, it is important to note that applying a similar clear-sky sampling to the satellite data, ERA40 OLRc showed excellent agreement with CERES data and are thought to be realistic [Allan and Ringer, 2003; Allan et al., 2004]. The agreement between SRB and ERA-40 improves confidence in the quality of their respective OLRc climatologies.

[24] The tropical multiannual mean SNLc is considered in Figure 3. In addition to NCEP, ERA40 and SRB, the empirical estimate based on Prata [1996] and SSM/I data are also considered over the tropical oceans. Since the surface longwave emission is greater than the downward atmospheric emission for the climatological domain considered, SNLc is negative, representing a net heating of the atmosphere. This heating (negative cooling) is minimum

Table 1. Mean Clear-Sky Longwave Radiative Cooling of the Atmosphere and Spatial Standard Deviation (in Parentheses) for 1988–1994 Climatology

Data Set	Q_{LWc} , W m^{-2}	OLRc, W m^{-2}	SNLc, W m^{-2}
Global			
NCEP	182.6 (41.3)	268.6 (39.5)	−86.0 (12.4)
ERA40	183.5 (41.5)	265.1 (42.1)	−81.6 (15.0)
SRB	176.6 (38.5)	263.1 (42.5)	−86.5 (17.3)
Tropical			
NCEP	210.0 (13.7)	290.0 (6.6)	−80.1 (15.1)
ERA40	212.8 (16.5)	286.7 (7.6)	−73.9 (17.4)
SRB	202.6 (18.8)	285.0 (7.2)	−82.5 (21.5)
Tropical oceans			
NCEP	213.1 (9.8)	290.0 (4.5)	−76.9 (8.9)
ERA40	216.9 (11.8)	287.5 (6.1)	−70.6 (11.8)
SRB	208.2 (11.2)	285.3 (4.9)	−77.1 (11.8)
Prata-SSM/I			−64.3 (11.3)

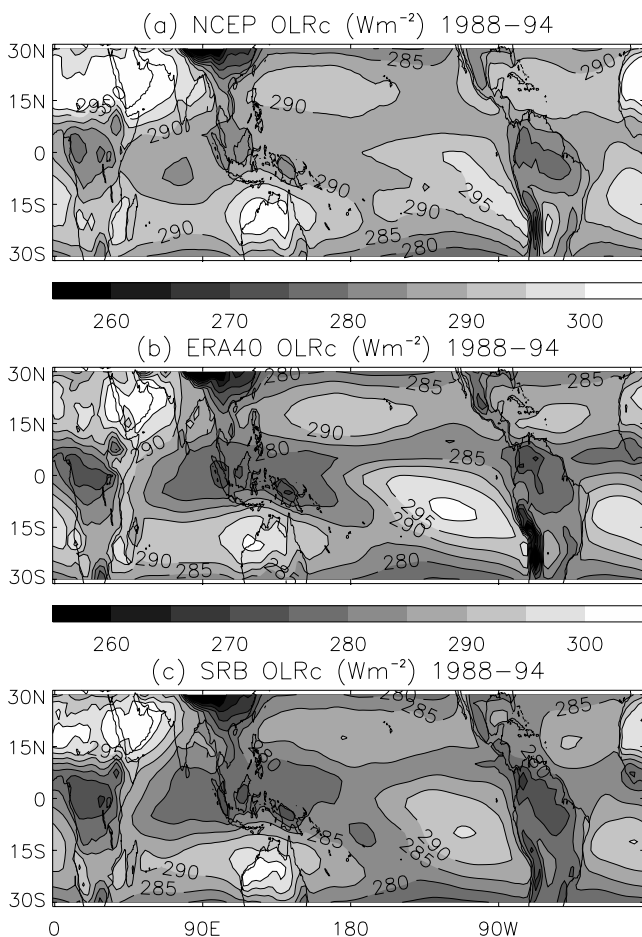


Figure 2. Mean clear-sky outgoing longwave radiation (OLRc) for (a) NCEP, (b) ERA40 and (c) SRB over the period 1988–1994.

over the tropical west Pacific where the high water vapor amounts cause saturation over much of the longwave radiation spectrum. Heating increases over the cool stratocumulus regions where the atmosphere is relatively dry. This is captured by all data sets considered, including the empirical method. However, the spatial distributions of SNLc appear less coherent in the NCEP data.

[25] Over the tropical oceans, NCEP and SRB data produce the strongest surface atmospheric heating (SNLc $\sim -77 \text{ W m}^{-2}$) while ERA40 data give values of SNLc $\sim 6 \text{ W m}^{-2}$ more positive (less atmospheric heating) than NCEP or SRB (Table 1). The empirical formula gives a value of SNLc a further 6.3 W m^{-2} more positive than the ERA40 data (SNLc $\sim -64 \text{ W m}^{-2}$). Over land, the SRB data produces the most negative values of SNLc with values less than -160 W m^{-2} over parts of northern Africa (white contour in Figure 3). This strong net heating of the atmosphere by the surface in SRB explains the low values of Q_{LWc} found over this region in Figure 1c.

[26] Since surface emissivity is observationally based in SRB but assumed fixed at unity in NCEP, errors in ϵ_s may influence the accuracy of SNLc in this region. Considering equation (1) and assuming typical conditions for the Sahara ($\epsilon_s = 0.9$ and $SDLc - \sigma T_s^4 = -150 \text{ W m}^{-2}$) it is likely that NCEP will produce SNLc approximately 15 W m^{-2} more

negative than SRB over this region. This is of the opposite sign required to explain the lower SRB estimates of SNLc and Q_{LWc} for this region. Another possibility is aerosol; climatological aerosol is prescribed for NCEP and ERA40 but are not considered for the longwave calculations of SRB. The inclusion of aerosol will reduce the magnitude of surface longwave cooling. This effect is, however, not large enough to fully explain the $\sim 10\text{--}30 \text{ W m}^{-2}$ more negative SNLc found over land regions in SRB. Errors in near-surface temperature and humidity profiles are likely to contribute to these differences.

[27] The global mean estimates of Q_{LWc} in Table 1 are over $20\text{--}30 \text{ W m}^{-2}$ higher than estimates from Kiehl and Trenberth [1997] ($Q_{LWc} = 153 \text{ W m}^{-2}$). While OLRc estimates agree well, Kiehl and Trenberth [1997] find a global mean SNLc of -112 W m^{-2} , significantly more negative than calculated from the data sets used in the present study. This is consistent with results from Wild *et al.* [2001] who used surface observations of longwave fluxes to show that many general circulation models and reanalyses underestimated the SDLc, therefore simulating values of SNLc that are too negative, because of deficiencies in the radiative transfer codes in particular for higher latitudes.

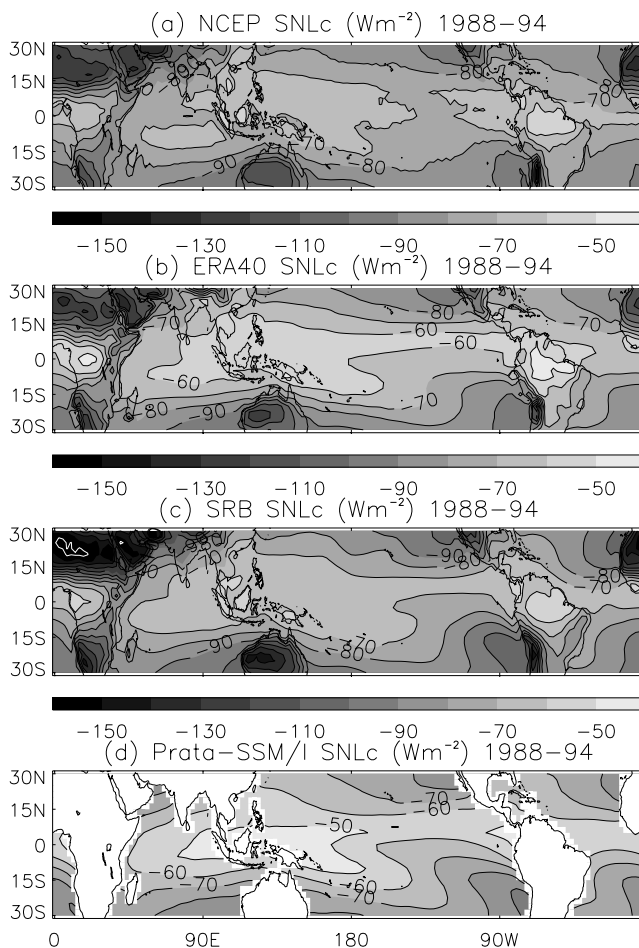


Figure 3. Mean clear-sky surface net longwave radiation (SNLc) for (a) NCEP, (b) ERA40, (c) SRB and (d) the Prata formula using SSM/I *CWV* ocean data over the period 1988–2004. A white contour in Figure 3c denotes SNLc = -160 W m^{-2} .

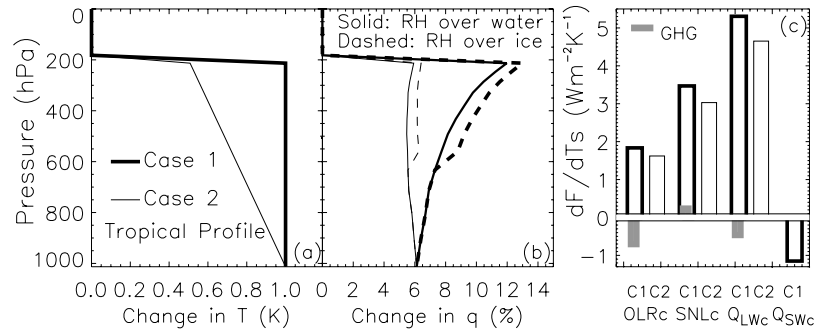


Figure 4. Details of sensitivity study conducted using a tropical standard atmospheric profile: (a) temperature perturbations for case 1 (C1) and case 2 (C2) with atmospheric pressure (p); (b) specific humidity (q) changes expressed as a percentage of the initial $q(p)$ profile calculated from temperature perturbations and assuming constant relative humidity (RH) computed separately with respect to water and ice; and (c) the changes in clear-sky OLR (OLRc), clear-sky surface net downward longwave radiation (SNLc), clear-sky atmospheric longwave radiative cooling (Q_{LWc}) and clear-sky atmospheric shortwave cooling (Q_{SWc}) calculated for C1 (thick) and C2 (thin). Also shown are the changes in longwave fluxes due to increased CO_2 , CH_4 , N_2O , CFC-11 and CFC-12 over the period 1980–2000 (gray).

[28] In summary, the NCEP data appear to produce an unrealistic distribution in clear-sky longwave radiative fluxes at the surface and top of the atmosphere as found previously [Allan *et al.*, 2004]. ERA40 simulates the strongest atmospheric clear-sky longwave cooling. Clear-sky OLR from ERA40 is thought to be realistic [Allan *et al.*, 2004] and agrees well with SRB; the high Q_{LWc} from ERA40 instead originates from a less negative SNLc than NCEP and SRB. Since the SNLc is strongly determined by CWV, and the spatial distribution of CWV simulated by ERA40 is realistic over the ocean [Allan *et al.*, 2004; Trenberth *et al.*, 2005] there is no reason to suspect that ERA40 overestimates the SNLc here. This case is strengthened by considering that the empirical formula, based on observational data over the ocean, gives better agreement with ERA40 than with the remaining data sets. On the basis of this reasoning it is suggested that the climatological simulation of Q_{LWc} from ERA40 is likely to be superior to SRB and NCEP.

4. Variability in Clear-Sky Radiative Cooling 1979–2004

[29] The variability of Q_{LWc} and its determinant variables are now considered over the period 1979–2004 for the data sets detailed in section 2. The primary aims of this section are (1) to intercompare the different estimates of Q_{LWc} variability, (2) to quantify relationships between variables important in determining Q_{LWc} , and (3) to understand what determines variability in Q_{LWc} over interannual to decadal timescales.

4.1. Sensitivity Study

[30] As a framework for interpreting the changes in clear-sky longwave cooling, a series of sensitivity studies were first undertaken using the *Edwards and Slingo* [1996] radiation scheme. Two experiments were performed using a tropical mean profile from *McClatchey et al.* [1972]. For each experiment, a warming was applied for pressure, $p \geq 200$ hPa and the water vapor concentrations were increased

such that the relative humidity (RH) remained constant. This is a reasonable assumption based on modeling and observational evidence [Soden *et al.*, 2005].

[31] The two scenarios considered (Figure 4a) are (1) C1 (thick line), an increase in temperature (dT) of 1 K for $p \geq 200$ hPa, and (2) C2 (thin line), an increase in 1 K at the surface and a reduced temperature increase aloft described by,

$$dT = \frac{p - p_{200}}{2(p_s - p_{200})} + 0.5, \quad (5)$$

where p_s is the surface level pressure (hPa) and $p_{200} = 200$ hPa.

[32] For both C1 and C2, $dT(p < 200 \text{ hPa}) = 0$. These scenarios were chosen to approximate differing interannual relationships from two general circulation models [Allan *et al.*, 2002]. The 1 K surface warming applied is of similar magnitude to the range of tropical mean interannual variability (e.g., see Figure 7). The resulting fractional change in specific humidity (q), assuming RH was calculated with respect to water, is displayed in Figure 4b (solid lines). Also shown are calculations where RH is calculated with respect to ice for temperatures less than 0°C (dotted lines).

[33] Radiative computations were performed on each scenario, setting trace gas values to the values currently used in the Met Office global forecast model (UKMO in Table 2). Figure 4c shows the changes in OLRc, SNLc and Q_{LWc} for cases C1 and C2. The effect of calculating RH with respect to ice does not alter the radiative flux changes

Table 2. Greenhouse Gas Concentration (by Mass) Used in the Radiative Transfer Calculations^a

Trace Gas	CO_2 , ppm	CH_4 , ppb	N_2O , ppb	CFC-11, ppb	CFC-12, ppb
1980	517	869	461	0.75	1.24
2000	562	970	479	1.23	2.24
UKMO	524	914	467	1.05	1.60

^aTo convert to volume mixing ratio, multiply by (molecular mass of dry air)/(molecular mass).

by more than 10% and so are not plotted. There is only a small difference (about 10%) in OLRc response to the two warming scenarios which increases at around $1.7 \text{ W m}^{-2} \text{ K}^{-1}$; a similar result was found from analysis of interannual variability in two climate model simulations [Allan *et al.*, 2002]. Although the warming in C1 is largest (increased OLRc), the water vapor increases are also largest (reduced OLRc) and so the OLRc is relatively insensitive to changes in temperature lapse rate provided that RH remains constant, as found previously by Cess [1975].

[34] The radiative response at the surface is slightly more marked than at the top of the atmosphere with C1 producing an increase in SNLc of $3.5 \text{ W m}^{-2} \text{ K}^{-1}$, about 14% larger than in C2. Note that the surface is less able to cool in the longwave spectrum for clear skies under the warming scenarios; this has also been demonstrated using surface observations [e.g., Lubin, 1994]. Both warming scenarios therefore increase the clear-sky longwave radiative cooling by increased emission to space and, to a greater extent, the surface, with the total atmospheric cooling, Q_{LWc} , ranging from $4.7 \text{ W m}^{-2} \text{ K}^{-1}$ (C2) to $5.3 \text{ W m}^{-2} \text{ K}^{-1}$ (C1).

[35] As noted in section 1, increases in water vapor also affect the clear-sky atmospheric shortwave radiative heating (Q_{SWc} , defined here as a negative cooling). A typical ocean surface albedo of 0.05 was prescribed. Solar zenith angle was set to 60° and a top of atmosphere insolation of 800 W m^{-2} applied to represent daytime conditions; this ensures a mean (day plus night) insolation of 400 W m^{-2} , typical of the tropical mean. The changes in Q_{SWc} were calculated on the basis of scenario C1 to offset the increases in Q_{LWc} by about 20% (Figure 4c), mainly through decreased insolation at the surface.

[36] A final experiment was performed with the tropical profile in which trace gas concentrations were increased from values representative of 1980 to concentrations typical of 2000 (Table 2) based in part on observations from the ALE/GAGE/AGAGE network [Prinn *et al.*, 2000]. Changes in ozone were not considered in the present study; a climatological tropical profile was prescribed from McClatchey *et al.* [1972]. Applying the change in trace gases reduces Q_{LWc} by 0.5 W m^{-2} because of reduced OLRc, offset by a small increase in emission to the surface. The reduction in OLRc offsets the OLRc increases for C1 by almost 40%. On the basis of these calculations, the OLRc increase due to a warming of 0.2 K per decade would be cancelled out by current increases in trace gas concentrations.

[37] In summary, tropospheric warming under constant RH results in a strong increase in Q_{LWc} of around $5 \text{ W m}^{-2} \text{ K}^{-1}$, the majority of which is due to increased downward emission to the surface. This is estimated to be offset by about $1 \text{ W m}^{-2} \text{ K}^{-1}$ because of increased shortwave absorption by water vapor and also by rising trace-gas concentrations which act to reduce Q_{LWc} by $\sim 0.25 \text{ W m}^{-2} \text{ decade}^{-1}$. These results relate to idealized sensitivity studies and are not presented as accurate predictions of changes in radiative cooling. Nevertheless they provide a useful means for interpreting the observed and simulated variability in Q_{LWc} presented in the following sections.

4.2. Global and Tropical Variations

[38] Global monthly mean variability in Q_{LWc} and its determinant variables are now considered for the reanalysis

data sets over the period 1979–2004. Interannual and decadal fluctuations are analyzed by removing the mean seasonal cycle from each time series. The time series are presented in Figure 5 while relationships between the variables are plotted in Figure 6. Linear regression between selected variables (CWV, SNLc, OLRc, Q_{LWc}) and T_s are displayed in Table 3 for each time series. Statistical uncertainty is represented by plus or minus one standard error. An asterisk denotes that the correlation coefficient is significant at the 95% level, allowing for autocorrelation of the data using the method of Yang and Tung [1998].

[39] Figure 5a shows interannual monthly anomalies of T_s . The ERA40 and NCEP data sets show good agreement with a general warming trend over the period, punctuated by interannual variability. The SRB data show 0.2 K more positive anomalies over the period 1984–1986 because of warmer conditions over polar and continental regions. The variability in CWV (Figure 5b) is markedly different between ERA40 and NCEP as documented previously [Allan *et al.*, 2004; Trenberth *et al.*, 2005] with a stronger apparent dependence on T_s in ERA40 than NCEP (Figure 6a and Table 3).

[40] The time series of SNLc (Figure 5c) show similarity to the CWV variations in Figure 5b, highlighting the strong dependence of SNLc on CWV (Figure 6e) with the approximate relationship, $d\text{SNLc}/d\text{CWV} \sim 1.5 \text{ W kg}^{-1}$. Because warming of surface and near-surface layers increase both the downward and upward surface longwave radiation, the SNLc is primarily sensitive to changes in atmospheric emissivity which in turn is highly sensitive to CWV (see Prata [1996] and equations (1) and (2)). It thus follows that errors in CWV will also impact SNLc and Q_{LWc} . For example, the anomalously low CWV at the beginning of 1980 in the ERA40 data corresponds with a negative anomaly in the SNLc record. A positive anomaly is also present at this time in the ERA40 OLRc time series (Figure 5d) but not in the temperature record. This is symptomatic of a positive RH bias in ERA40 which acts to reduce atmospheric cooling to space but increases cooling to the surface. This compensation explains the lack of anomaly in the Q_{LWc} record for ERA40 for this period.

[41] The OLRc variability shows large differences between data sets. ERA40 produces positive OLRc anomalies during the period 1986–1991 and negative anomalies after 1997 compared to NCEP. Again, it is likely that OLRc variability is affected by changes in the reanalysis observing systems [Allan *et al.*, 2004]. ERA40 and SRB show a larger variation in SNLc than OLRc which explains why the global changes in total atmospheric cooling, Q_{LWc} , are primarily explained by the surface cooling component (Figure 6f).

[42] Despite the large differences in variability of CWV, SNLc and OLRc between data sets, agreement between interannual anomalies in Q_{LWc} (Figure 5e) appears more robust. Both NCEP and ERA40 capture the large increase in all variables considered in Figure 5 during the 1997–1998 El Niño event. ERA40 shows more negative anomalies than NCEP during 1980 and 1985 because of differences in the surface rather than top of atmosphere component of Q_{LWc} . ERA40 produces anomalies up to 1 W m^{-2} more positive than NCEP during the period 1992–1996. However, throughout the remainder of the record, differences in OLRc

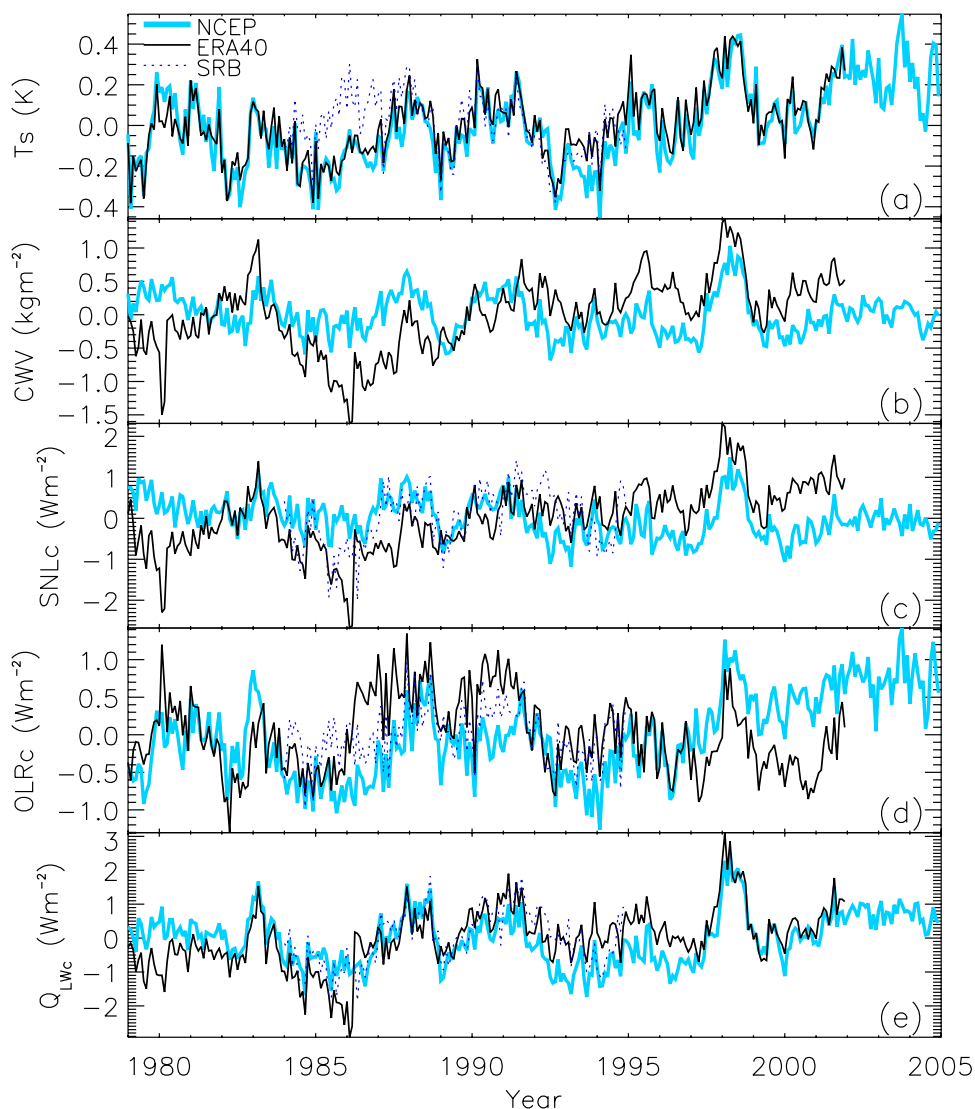


Figure 5. Time series of global monthly mean (a) surface temperature, (b) column integrated water vapor, (c) surface net downward longwave radiation, (d) clear-sky outgoing longwave radiation and (e) clear-sky atmospheric longwave radiative cooling over the period 1979–2004 with the mean annual cycle removed.

and SNLc anomalies compensate in terms of the total atmospheric longwave cooling (for example, the period 1998–2001). This is possible if a relative humidity error applies to the entire troposphere leading to compensating effects on the atmospheric cooling to space and to the surface [e.g., *Allen and Ingram, 2002; Mitchell et al., 1987*]. If, however, humidity errors affect only the lower or upper troposphere, this compensation will not arise since the OLRc is sensitive mainly to humidity in the mid and upper troposphere while the SNLc is primarily sensitive to boundary layer humidity.

[43] There is a robust relationship between Q_{LWc} and T_s for both ERA40 and NCEP (Figure 6d). ERA40 displays a $1 \text{ W m}^{-2} \text{ K}^{-1}$ larger increase in Q_{LWc} with T_s than NCEP (Table 3); this is due to a $2 \text{ W m}^{-2} \text{ K}^{-1}$ larger $d\text{SNLc}/dT_s$ which is offset by a $1 \text{ W m}^{-2} \text{ K}^{-1}$ smaller $d\text{OLRc}/dT_s$ response in ERA40. In general, all the variables considered show a positive relationship with surface temperature on

interannual timescales (Figure 6) although the correlation between SNLc and T_s is not statistically significant for the NCEP data. The SRB data produces a much smaller sensitivity to T_s which may be due to the shorter time period considered. However, ERA40 and NCEP sensitivities calculated for the SRB period are not statistically different at the 95% level to the sensitivities calculated over the entire period (not shown).

[44] Figure 6 illustrates how the positive global relationship between Q_{LWc} and T_s arises using the reanalysis data. There is a significant, positive dependence of CWV on T_s of $1.7 \text{ kg m}^{-2} \text{ K}^{-1}$ from ERA40, consistent with previous estimates from an atmosphere-only climate model and a fully coupled climate model of $1.4\text{--}1.8 \text{ kg m}^{-2} \text{ K}^{-1}$ [*Slingo et al., 2000*] and more than double the NCEP sensitivity. This positive relationship drives a corresponding increase in SNLc with surface warming (Figure 6c) due to the dominating effect of changes in water vapor on the SNLc (Figure 6e).

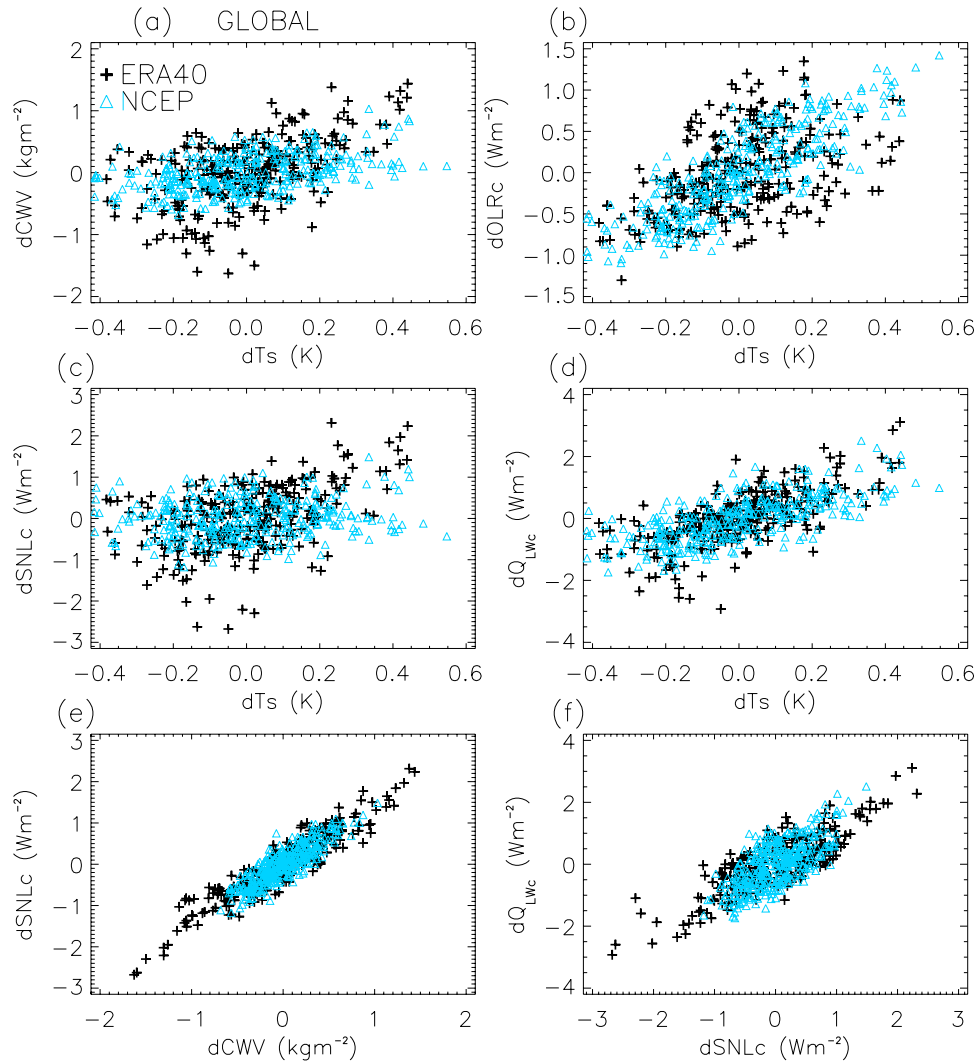


Figure 6. (a–f) Scatterplots of variables described in Figure 5 for ERA40 and NCEP over the period 1979–2001.

The large range in variation in the longwave radiative cooling of the atmosphere to the surface thus ensures a strong influence on Q_{LWc} (Figure 6f).

[45] Significant increases in global monthly mean OLRc with surface warming are also found for ERA40 and NCEP (Figure 6b). *Slingo et al.* [2000] also found a significant positive relationship between OLRc and T_s of 1.9 to $2.4 \text{ W m}^{-2} \text{ K}^{-1}$ for a range of models and reanalyses, consistent with the NCEP sensitivity but larger than the ERA40 sensitivity displayed in Table 3. When output from a coupled model, including greenhouse gas forcing, was considered by *Slingo et al.* [2000], the relationship between OLRc and T_s was insignificant. This was because the warming in the coupled model experiment that contributed to increased OLRc was associated with increased greenhouse gas concentration which counteracted this OLRc increase. When the coupled model sensitivity was recalculated with unchanging greenhouse gas concentrations, a sensitivity of $1.7 \text{ W m}^{-2} \text{ K}^{-1}$ was calculated [*Slingo et al.*, 2000]. While the coupling between surface temperature and greenhouse gas concentration is smaller on the shorter

timescales considered in the present analysis, the sensitivity study performed in section 4.1 also demonstrated that decadal increases in greenhouse gases may significantly offset increases in OLRc with warming. Since realistic changes in global mean greenhouse gas concentrations are prescribed in ERA40 but are held fixed in NCEP, this may contribute to the lower OLRc sensitivity to T_s found in ERA40. The increases in cooling to the surface due to increased water vapor (Figures 6a and 6c) and the greater emission to space with tropospheric warming under constant relative humidity (positive $dOLRc/dT_s$; Figure 6b) explain the robust relationship between clear-sky longwave radiative cooling of the atmosphere and surface temperature (Figure 6d).

[46] Time series for the tropical domain (30°S – 30°N) are similar in nature to the global comparisons and so are not shown. However, interannual anomalies are generally larger and decadal trends smaller for the tropical region compared with the global comparisons. Correlation with T_s is also stronger for the tropical region (Table 3). The sensitivity of Q_{LWc} to T_s of $5.1 \text{ W m}^{-2} \text{ K}^{-1}$ for NCEP and $5.6 \text{ W m}^{-2} \text{ K}^{-1}$

Table 3. Linear Regression Analysis of CWV, SNLc, OLRc and Q_{LWc} With T_s Over Global and Tropical Domains for the ERA40, NCEP, SRB and OBS Data Sets Calculated for the Temporal Coverage of Each Data Set^a

	Period ^a	$\frac{dCWV}{dT_s}$, kg m ⁻² K ⁻¹	$\frac{dSNLc}{dT_s}$, W m ⁻² K ⁻¹	$\frac{dOLRc}{dT_s}$, W m ⁻² K ⁻¹	$\frac{dQ_{LWc}}{dT_s}$, W m ⁻² K ⁻¹
Global					
ERA40	1979–2001	1.7 ± 0.2*	2.3 ± 0.3*	1.4 ± 0.2*	3.7 ± 0.2*
NCEP	1979–2004	0.7 ± 0.1*	0.4 ± 0.1	2.4 ± 0.1*	2.7 ± 0.2*
SRB	1984–1994		−0.6 ± 0.4	1.3 ± 0.2*	0.7 ± 0.5
Tropical					
ERA40	1979–2001	2.8 ± 0.3*	3.5 ± 0.4*	2.2 ± 0.3*	5.6 ± 0.3*
NCEP	1979–2004	2.0 ± 0.1*	2.5 ± 0.2*	2.6 ± 0.2*	5.1 ± 0.2*
SRB	1984–1994		0.4 ± 0.5	1.4 ± 0.2*	1.9 ± 0.6
Tropical ocean					
ERA40	1979–2001	2.7 ± 0.5	3.5 ± 0.6	2.7 ± 0.3*	6.2 ± 0.5*
NCEP	1979–2004	2.0 ± 0.2*	2.5 ± 0.2*	2.7 ± 0.2*	5.2 ± 0.3*
SRB	1984–1994		3.7 ± 0.4*	1.2 ± 0.3*	4.8 ± 0.4*
OBS ^a	1979–2004	3.0 ± 0.1*	2.9 ± 0.2*	0.5 ± 0.4	3.6 ± 0.5*
Tropical ocean: ascent					
ERA40	1979–2001	5.5 ± 0.4*	6.2 ± 0.4*	−0.1 ± 0.3	6.1 ± 0.3*
NCEP	1979–2004	2.8 ± 0.2*	3.0 ± 0.3*	1.7 ± 0.2*	4.6 ± 0.2*
SRB	1984–1994		4.6 ± 0.3*	0.2 ± 0.2	4.8 ± 0.3*
OBS ^a	1979–2001	4.1 ± 0.2*	4.0 ± 0.2*	0.2 ± 0.6	4.8 ± 0.5*
Tropical ocean: descent					
ERA40	1979–2001	1.1 ± 0.3	1.1 ± 0.5	2.6 ± 0.3*	3.7 ± 0.5*
NCEP	1979–2004	1.4 ± 0.2*	1.8 ± 0.2*	2.4 ± 0.2*	4.2 ± 0.3*
SRB	1984–1994		3.0 ± 0.4*	0.6 ± 0.4	3.6 ± 0.4*
OBS ^a	1979–2001	2.1 ± 0.1*	2.2 ± 0.2*	2.8 ± 0.4*	4.6 ± 0.4*

^aThe time periods used are stated in column 2. OBS denotes combination of SMMR-SSM/I for CWV and the *Prata* [1996] formula using HadISST/da Silva T_0 and SMMR-SSM/I CWV for SNLc (no data for 1985–1986); ERBS, ScaRaB and CERES were used for OLRc (no data 1979–1984, 1990–1993, 1996–1997 and 1999) and a combination of all listed sources for Q_{LWc} (no data 1979–1986, 1990–1993, 1996–1997 and 1999). Asterisks denote values that are significant at the 95% confidence level accounting for autocorrelation.

for ERA40 is comparable with the idealized sensitivity test, C1, shown in Figure 4. This suggests that interannual variability may conform to the simple model of constant relative humidity and temperature lapse rate detailed in section 4.1. The calculated SRB sensitivity $dQ_{LWc}/dT_s = 1.9 \text{ W m}^{-2} \text{ K}^{-1}$, is less than ERA40 and NCEP, even when calculated over the same period (1984–1994), and is not statistically significant.

4.3. Observed and Simulated Relationships Over the Tropical Oceans

[47] The tropical ocean domain is now analyzed in detail using the observational data sets as well as the reanalyses. Deseasonalized anomalies are calculated by removing the mean seasonal cycle based on the available temporal coverage. Figure 7a shows the sea surface temperature anomalies from ERA40, NCEP, SRB and HadISST over the period 1979–2004. There is good agreement (to within 0.1 K) although HadISST shows cooler anomalies than NCEP and ERA40 from the end of 1979 to the beginning of 1980. The range in T_s anomalies reaches nearly 1 K, mainly because of changes in the atmosphere-ocean circulations relating to the El Niño Southern Oscillation (ENSO).

[48] The CWV variability depicted by NCEP data shows close correspondence with observations from SMMR and SSM/I (Figure 7b) while ERA40 shows anomalous variability as noted previously [Allan *et al.*, 2004]. Again, the February–March 1980 anomalies are present for the ERA40 data indicating humidity errors over the tropical ocean. There is a closer correspondence between CWV variability and T_s over the tropical oceans than for the global comparison. This is because (1) the tropics are warmer and so a change in temperature produces a larger

change in water vapor concentrations for a given relative humidity and (2) the greater availability of water over the oceans compared to land. Correlations between CWV and T_s appear stronger for NCEP than ERA40 (Figure 8a); although $dCWV/dT_s$ is larger for ERA40 (Table 3) the linear fit is not statistically significant because of a large scatter. The observed sensitivity, $dCWV/dT_s = 3 \text{ kg m}^{-2} \text{ K}^{-1}$ for the SMMR-SSM/I and HadISST data, provides the most robust relationship (Figure 9a) and is consistent with an estimate from a coupled climate model for the global ice-free oceans [Slingo *et al.*, 2000], but larger than the NCEP sensitivity.

[49] The tropical variability of SNLc over the oceans (Figure 7c) again shows similarity to CWV variability. The empirical estimate of SNLc using observational data produces a similar variation and sensitivity to the NCEP record (Table 3) despite the different approaches used. The variability in SNLc from all data sets considered is smaller than the range in tropical mean anomalies of net longwave flux of -5 to $+7 \text{ W m}^{-2}$ estimated by Soden [2000] over the period 1983–1991. Although this implies a large cloud effect on the surface net flux, it is not clear how accurate the all-sky estimates are. Calculations made by Pavlakis *et al.* [2004] of all-sky downward longwave flux for the northern and southern hemisphere show a smaller range ($\sim 2 \text{ W m}^{-2}$) over the period 1984–1993. However, the downward longwave flux variability is generally larger than the net longwave flux since changes in upward emission due to temperature changes are strongly compensated by changes in downward emission if the atmospheric temperature is coupled to T_s . Indeed, global anomalies in SDLc for NCEP vary by $\sim \pm 2-3 \text{ W m}^{-2}$, similar to the estimate from Pavlakis *et al.* [2004], and approximately double the variation in NCEP SNLc.

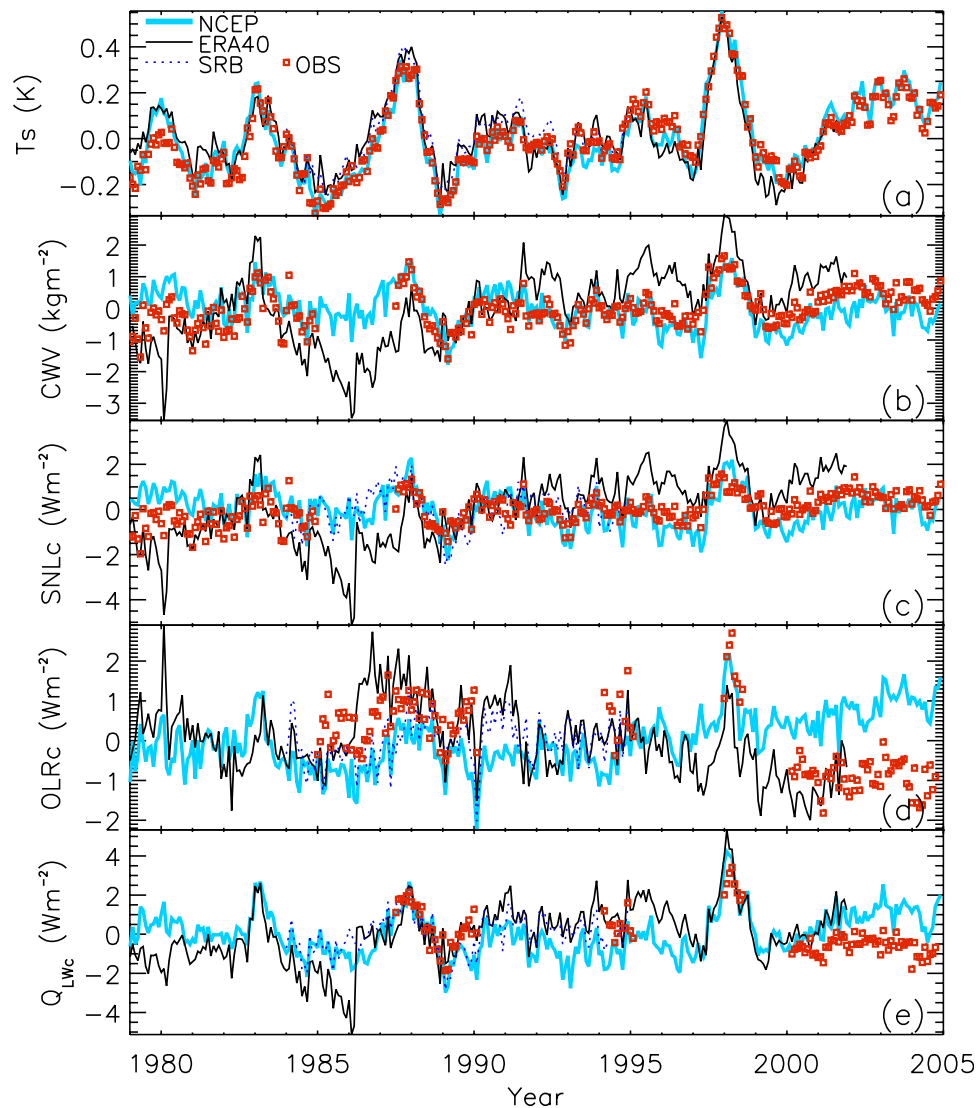


Figure 7. As Figure 5 but for the tropical oceans. In addition to ERA40, NCEP and SRB products there is observational and empirical data (OBS) comprising (a) HadISST ocean surface temperature; (b) column integrated water vapor from SMMR and SSM/I; (c) the Prata formula estimate of SNLc using SMMR and SSM/I data; (d) radiation budget satellite data from ERBS (1985–1990), ScaRaB (1994/1995), CERES on TRMM (1998) and CERES on TERRA (2000–2004); and (e) combined ERBS/ScaRaB/CERES and Prata-SSM/I estimates of SNLc.

[50] Variations in OLRc (Figure 7d) between NCEP and ERA40 show substantial differences despite a similar sensitivity, $dOLRc/dT_s = 2.7 \text{ W m}^{-2} \text{ K}^{-1}$. Indeed, the period 1986–2001 is characterized by a positive trend in NCEP OLRc and a negative trend from ERA40. This sensitivity is larger than estimated from a range of climate model experiments over the global ice-free oceans [Slingo *et al.*, 2000] and also the estimates from SRB and the satellite data record (OBS) in Figure 7d. As discussed in section 3, there is a difference in sampling between the satellite clear-sky data and reanalyses/models which causes an apparent bias in the climatology. As shown by Allan *et al.* [2003], the different sampling does not affect the anomaly time series although the caveat remains that the satellite data are sampling generally more suppressed, clear-sky situations relative to the reanalyses. This may affect the comparisons

if there is a large difference in response of the descending and ascending portions of the atmospheric circulation to warming.

[51] While the ERA40 OLRc appears anomalously high in 1986–1987, agreement with SRB, ERBS and ScaRaB anomalies appears better than NCEP over the subsequent period 1988–1995. During early 1997, there is a reduction in OLRc anomalies from ERA40 relative to NCEP; it is interesting that negative anomalies during 2000–2001 are evident in both the ERA40 and CERES-Terra data. It is not clear whether this is a real change in OLRc or a satellite calibration difference: absolute calibration uncertainty is estimated as about 0.5% [Wielicki *et al.*, 2002] or about 1.5 W m^{-2} of tropical mean OLRc, which is similar in magnitude to the interannual variability. An additional factor is the instrument pixel size with the

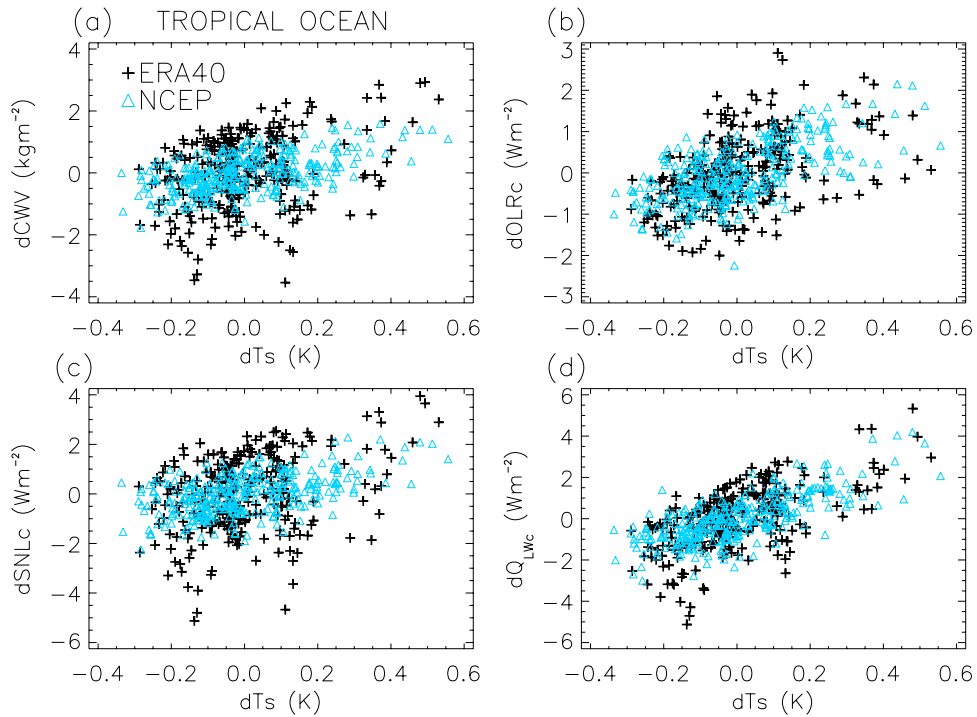


Figure 8. Scatterplots of monthly mean (a) column integrated water vapor, (b) clear-sky outgoing longwave radiation, (c) clear-sky surface net downward longwave radiation and (d) clear-sky atmospheric longwave radiative cooling with monthly mean surface temperature over the tropical oceans for ERA40 and NCEP over the period 1979–2001.

CERES instruments having higher spatial resolution and therefore identifying more clear-sky scenes than ERBS. Since smaller pixel sizes allow sampling of more moist, clear regions close to clouds, and these profiles produce lower OLRc, this could conceivably explain why TERRA

OLRc is lower than ERBS. However, this does not seem likely to explain the change in clear-sky OLR from CERES/TRMM to CERES/TERRA which are likely to be affected by real changes in temperature and humidity as well as calibration differences.

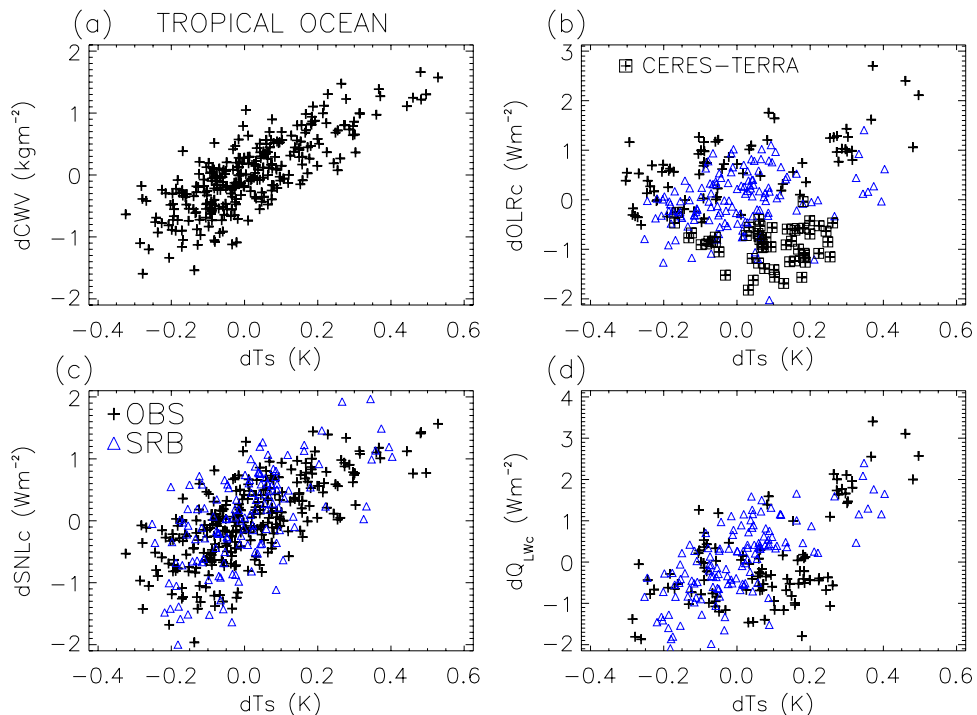


Figure 9. (a–d) As Figure 8 but for observed quantities described in Figure 7 and SRB data.

[52] The variations in Q_{LWc} for tropical oceans appear reasonably consistent between data sets as found for the global mean comparison of the reanalysis data. In particular the increase in Q_{LWc} during the ENSO warm events of 1982–1983, 1986–1987 and 1997–1998 are captured by the reanalyses and observationally based data. As suggested previously, errors in relative humidity exert opposite influences on the atmospheric cooling at the surface and the top of atmosphere, thereby reducing the impact on errors in Q_{LWc} . ERA40 simulates anomalies up to 2 W m^{-2} lower than NCEP and SRB during 1979 and 1985 while NCEP simulates anomalies around 1 W m^{-2} lower than the other data sets during the period 1992–1996. There is a rapid increase in Q_{LWc} anomalies of 5 W m^{-2} between March and April 1986 in the ERA40 data set, associated with increased CWV and SNLc. This is explained by a rise in lower tropospheric relative humidity of 1–2% compounded by a modest lower tropospheric warming in ERA40 (not shown). Corresponding with this time, there is also an increase in OLRc of nearly 1 W m^{-2} . This may be in part explained by the lower tropospheric warming and a reduction in relative humidity in the mid and upper troposphere although there is also a cooling in the upper troposphere and a moistening between 250–300 hPa which will act to reduce OLRc. These changes are likely to be unrealistic and an artifact of the reanalysis system.

[53] The sensitivity $dQ_{LWc}/dT_s \sim 5\text{--}6 \text{ W m}^{-2} \text{ K}^{-1}$ for ERA40, NCEP and SRB (Table 3), is in line with the idealized calculations presented in section 4.1. The observationally determined relationship of $3.6 \text{ W m}^{-2} \text{ K}^{-1}$ is somewhat smaller. This is primarily explained by a poor relationship between OLRc and T_s (Figure 9b) which in turn is caused mainly by the latest CERES observations of negative OLRc anomalies despite positive temperature anomalies during the period 2001–2004 (Figure 7a). The increase in tropical atmospheric longwave radiative cooling estimated from the observations therefore appears primarily driven by the enhanced cooling to the surface, determined by robust, positive relationship between low-level water vapor and surface temperature.

4.4. Ascending and Descending Portions of the Tropical Oceans

[54] To investigate further the relationships between radiative cooling and surface temperature and their differences between data sets, the tropical ocean is now subdivided into ascending and descending portions. This is accomplished by subsampling the data sets using 500 hPa vertical motion fields (ω). Grid points of negative monthly mean ω are defined as ascent regions while grid points with $\omega \geq 0$ are defined as descending. Clear-sky atmospheric radiative cooling to space (OLRc), while relevant for the descending regime which is predominantly free of deep cloud, is less applicable for the ascending regions where cloud is extensive. The relationships here are less likely to dominate the diabatic cooling and instead serve as an informative diagnostic. Vertical motion fields from ERA40 are used since these display a more realistic spatial distribution than NCEP values [e.g., Ringer and Allan, 2004]. However, NCEP vertical motion fields are used to subsample the NCEP data since these fields are self-consistent.

Anomaly time series and linear regression are applied to the resulting regimes.

[55] Time series of Q_{LWc} and determinant variables are displayed for the descending regime in Figure 10 and for the ascending regime in Figure 11. The anomalies in ERA40 data at the beginning of 1980 present in the global and tropical ocean comparisons originate in the descending regime while the decreasing OLRc trend from 1986–2001, apparent in the tropical comparison for both ERA40 and the satellite data, appears to stem from the ocean regions of mean ascent. However, the large increases in Q_{LWc} from March to April 1986 (and the anomalous record from 1985 to 1986) for ERA40 are present in both Figures 10e and 11e suggesting that the errors apply for the entire tropical ocean.

[56] The anomaly time series of SNLc are remarkably consistent between NCEP and the empirical estimate for the ascending regime, despite the differing approaches used in deriving this parameter. For both data sets, the calculated sensitivity $dCWV/dT_s$ over the ascending regime is approximately double that of the descending regime (Table 3). This arises because the ascending regime is warmer and more humid so for a given change in temperature and constant relative humidity, the change in water vapor holding capacity of the atmosphere is greater. The water vapor response to warming appears overestimated by ERA40 in the ascending regime while the correlation between CWV and T_s is not significant for the descending regime; here the CWV record in ERA40 shows large deviations from the other data sets over the period which are likely to be artifacts of the assimilation system [Allan et al., 2004]. Recent results from Uppala et al. [2005] suggest that the 24-hour forecasts from the ERA-40 reanalysis may provide a more realistic decadal variability in water vapor and the clear-sky radiation budget.

[57] Apart from the 1985–1986 period, the observed changes in OLRc are well represented by ERA40 when partitioning into ascending and descending portions of circulation. The NCEP record appears inferior, in particular the increasing trend toward the end of the period. There is no clear relationship between OLRc and T_s in the ascending regime for OBS, SRB and ERA40 although there remains a positive relationship for NCEP (Table 3). For the descending regime, $dOLRc/dT_s$ is consistent to within $0.4 \text{ W m}^{-2} \text{ K}^{-1}$ for ERA40, NCEP and OBS; the SRB correlation is not statistically significant. The robust nature of the observed changes in OLRc have yet to be established, in particular between different satellites such as ERBS and CERES.

[58] The surface and top of atmosphere contribution to the relationship between Q_{LWc} and T_s varies between all data set. For SRB, cooling to the surface dominates the Q_{LWc} response for both regimes considered while the OBS relationship is dominated by the surface contribution in the ascending regime and both the surface and top of atmosphere contribute to dQ_{LWc}/dT_s in the descending region. The majority of the NCEP and ERA-40 dQ_{LWc}/dT_s response is due to the surface contribution for the ascending region and the top of atmosphere response in the descending regime. The dQ_{LWc}/dT_s is larger for the ascending regime because of the greater response of CWV, and hence SNLc, to T_s . Nevertheless, for both the ascending and descending oceanic regimes, dQ_{LWc}/dT_s ranges from 3.6 to $4.8 \text{ W m}^{-2} \text{ K}^{-1}$ in all data sets apart from the ascending regime for ERA-40 which produces a larger response. It has been demonstrated

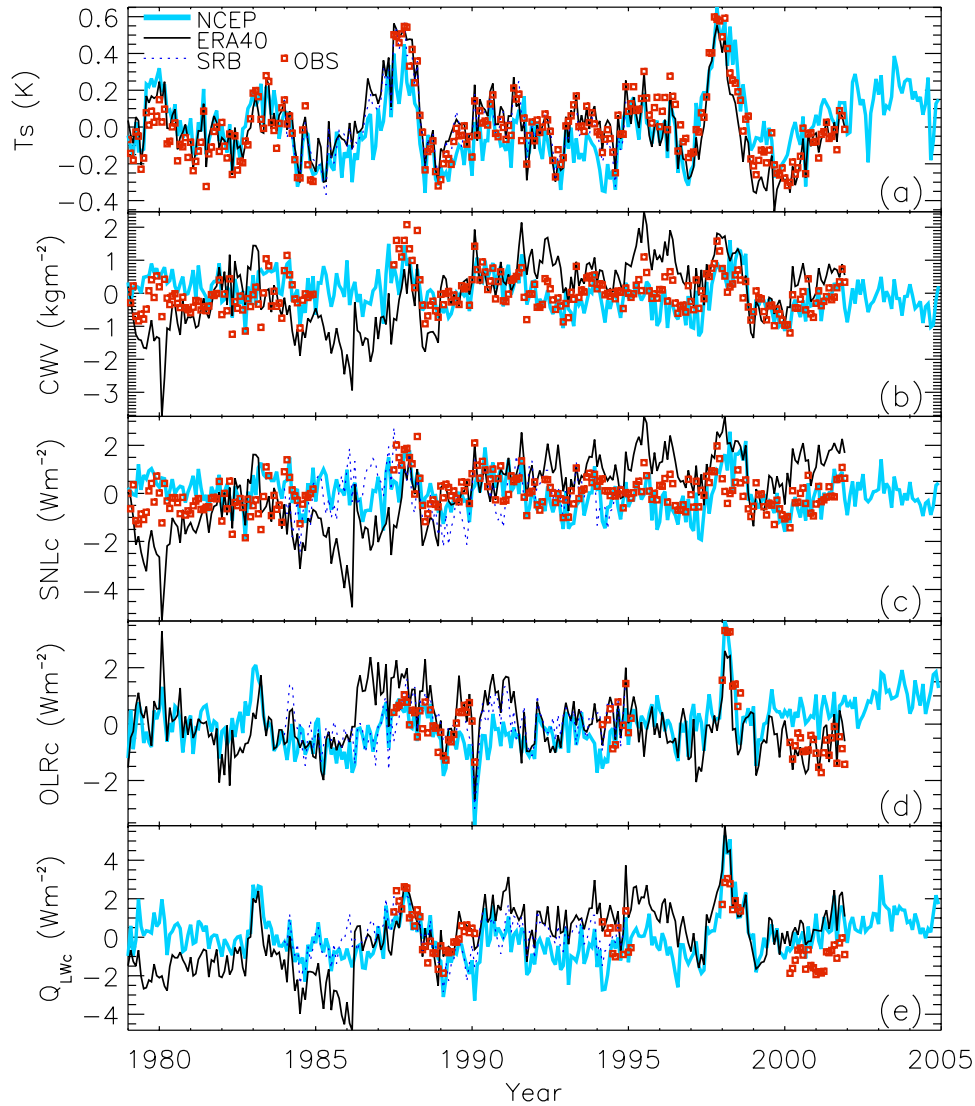


Figure 10. (a–e) As Figure 7 for grid points of monthly mean descent diagnosed using ERA40 500 hPa vertical motion.

that all data sets display a strongly positive relationship between clear-sky atmospheric longwave radiative cooling and surface temperature over a variety of timescales and spatial domains. This has important implications for changes in latent heating of the atmosphere and therefore the character of precipitation [e.g., Trenberth *et al.*, 2003; Allen and Ingram, 2002].

5. Discussion

[59] An important component of the tropical hydrological cycle is the balance between latent heat release over convective regions and radiative cooling over the predominantly clear-sky descending branches of the tropical circulation [e.g., Hartmann and Larson, 2002]. Since the atmospheric radiative cooling is largest in the predominantly clear-sky descending portions of the tropical circulation and the satellite clear-sky data is more representative over these regions, the calculated sensitivity range for the descending regimes, $dQ_{LWc}/dT_s = 3.6$ to $4.6 \pm 0.4 \text{ W m}^{-2} \text{ K}^{-1}$ from the

different data sets and time periods presented in Table 3 is particularly relevant for changes in precipitation. Assuming that the changes in clear-sky atmospheric radiative cooling over the descending portion of the Hadley circulation dominate the precipitation in the ascending regions of the atmospheric circulation, the following relationship applies:

$$\frac{dP}{dT_s} = \frac{f_A}{\rho_w L} \frac{dQ_{LWc}}{dT_s}, \quad (6)$$

where P is the precipitation rate (in m s^{-1} ; multiply by 8.64×10^7 to convert to mm day^{-1}), L is the latent heat of evaporation ($2.5 \times 10^6 \text{ J kg}^{-1}$), $f_A \sim 0.6$ is the fractional area of the descending regime, estimated from the 30°S – 30°N ERA40 monthly mean vertical motion fields, and ρ_w is the density of water. Therefore the range of dQ_{LWc}/dT_s suggests a contribution to tropical precipitation of 0.07 to 0.1 mm day^{-1} per K warming. Assuming a tropical mean precipitation rate of 3 mm day^{-1} this translates to $\sim 3\%$ K^{-1} . Assuming a mean tropical CWV of 38 kg m^{-2} , the observed relationship

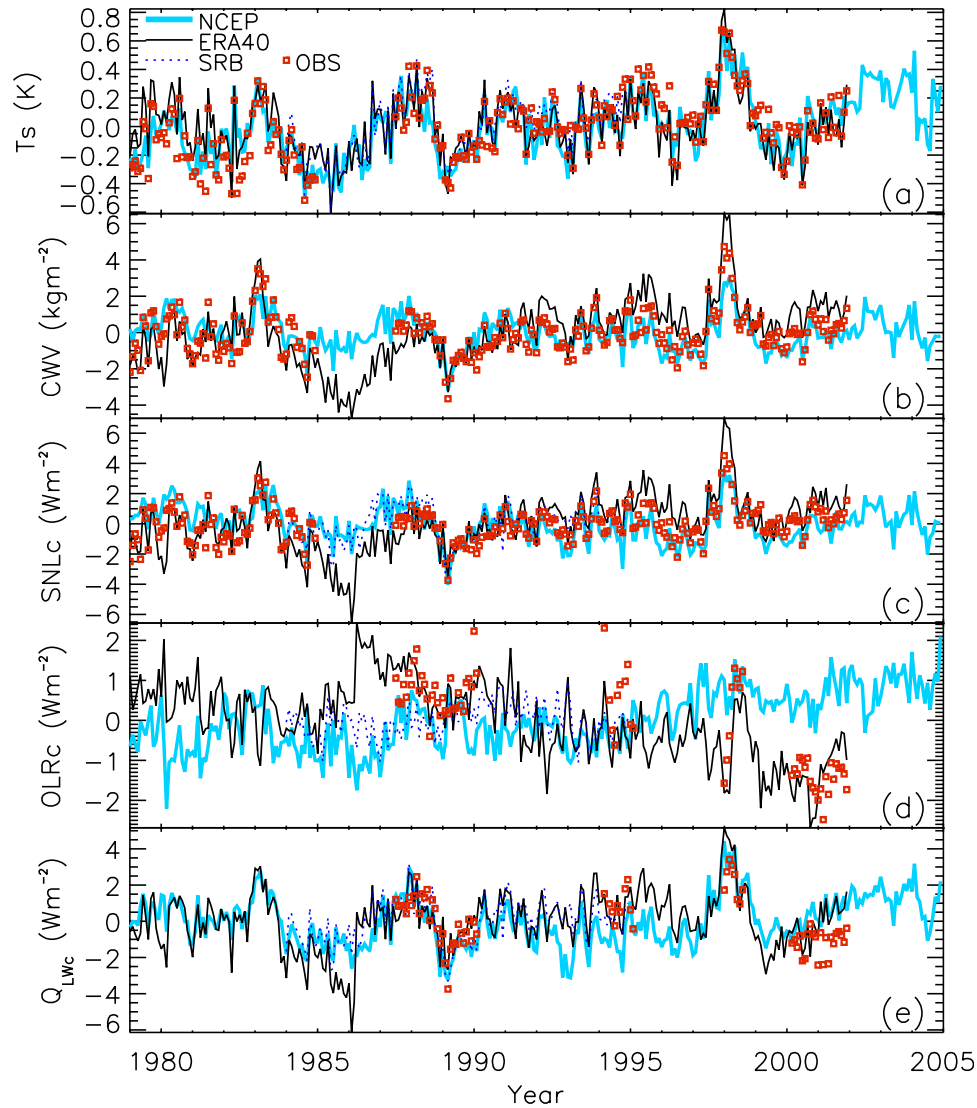


Figure 11. (a–e) As Figure 7 for grid points of monthly mean ascent diagnosed using ERA40 500 hPa vertical motion.

over the tropical oceans, $dCWV/dT_s = 3 \text{ kg m}^{-2} \text{ K}^{-1}$ translates to an increase of about $8\% \text{ K}^{-1}$. As discussed previously [e.g., Trenberth *et al.*, 2003; Allen and Ingram, 2002; Hartmann and Larson, 2002; Soden, 2000], this implies an increase in the water vapor residence timescale $\left(\frac{CWV}{\rho_w P}\right)$ suggesting more intense, less frequent precipitation. In future work it will be informative to compare changes in clear-sky and all-sky cooling with estimates of precipitation variability.

[60] The robust relationship between SNLc and CWV has been demonstrated on a variety of time and space scales. Since SNLc is an important component of the clear-sky atmospheric radiative cooling, CWV is therefore an important parameter in determining Q_{LWc} [e.g., Stephens *et al.*, 1994]. Over ascending regions of the tropical oceans, the positive relationship between Q_{LWc} and T_s arises because of the small increase in cooling to space and the large increase in cooling to the surface when tropospheric temperatures are increased but relative humidity is held fixed. Over descending regimes

of the tropical oceans, the strongly positive dQ_{LWc}/dT_s is explained both by increased cooling to the surface and to space with the increase in OLRc with warming tending to dominate.

[61] A column mean increase in relative humidity will have a small effect on Q_{LWc} since reductions in cooling to space are counteracted by increases in cooling to the surface [Allen and Ingram, 2002]. Combined with the increase in shortwave absorption with lower tropospheric humidity, it has been argued by Mitchell *et al.* [1987] that the atmospheric temperature changes dominate changes in clear-sky radiative cooling. Thus potential changes in relative humidity accompanying global warming, despite exerting a profound effect on the magnitude of water vapor feedback [e.g., Soden *et al.*, 2005], are likely to influence only marginally the changes in atmospheric radiative cooling, unless the relative humidity changes are restricted to a particular region of the troposphere. For example, increased upper tropospheric relative humidity will not directly affect

SNLc but will reduce OLRc although the resulting warming of the mid and lower troposphere are then able to indirectly influence cooling to the surface. In contrast the surface longwave radiation balance is sensitive to CWV rather than upper tropospheric humidity. Errors in relative humidity that apply throughout the column, however, will have only a marginal effect on the accuracy of Q_{LWc} . This is likely to explain why the spurious changes in water vapor and surface and top of atmosphere clear-sky radiation in ERA40 are less noticeable in the Q_{LWc} time series. It also suggests that monitoring both the CWV and upper tropospheric relative humidity is vital in understanding changes in the atmospheric hydrological cycle.

[62] There are a number of caveats to the analysis presented in the previous sections that are now discussed.

[63] 1. The effects of clouds are not included in the estimates of radiative cooling. It is likely that changes in cloudiness will strongly influence variability in atmospheric radiative cooling. *Soden* [2000] found an interannual variability range in tropical mean surface longwave flux greater than 10 W m^{-2} which was ascribed to boundary layer cloud. However, changes in downwelling longwave flux at the surface estimated by *Pavlakakis et al.* [2004] for all-sky conditions do not show a larger variability than those inferred from the present study for clear skies and at present agreement between satellite estimates of changes in cloudiness has not been established [*Wielicki et al.*, 2002; *Trenberth*, 2002; *Norris*, 2005; *Wylie et al.*, 2005]. Since changes in cloudiness are inextricably linked to precipitation it will be important to assess the clear and cloudy sky contribution to atmospheric radiative cooling in the future. However, it is paramount that such studies ensure that changes in the clear-sky radiation balance are robust to avoid misleading conclusions regarding the role of clouds on the radiation budget.

[64] 2. Clear-sky shortwave absorption by water vapor will also influence radiative cooling, as shown in section 4.1. Increased CWV will increase longwave cooling to the surface but increase atmospheric heating by shortwave absorption [e.g., *Mitchell et al.*, 1987]. Overall, the increase in Q_{LWc} with warming under constant relative humidity is estimated to be offset by shortwave radiation absorption by around 20% for tropical mean profiles. These estimates should be quantified more fully using global data. Also, since shortwave absorption will be larger during the day while not applying at night, this has implications for how the differential heating will affect the diurnal cycle of cloud, radiation and precipitation.

[65] 3. A further shortcoming of the present study is that atmospheric cooling can vary strongly with altitude. Cooling to space by OLRc primarily applies to the upper troposphere while cooling to the surface primarily affects the boundary layer. Therefore it is overly simplistic to treat the atmospheric radiative cooling as one term. The reanalyses and some observationally based data sets [e.g., *Zhang et al.*, 2004; *Slingo et al.*, 2000] allow analysis of the altitude-dependent changes in atmospheric cooling that may be explored.

[66] 4. The relationships gained from the present analysis are strongly influenced by ENSO variability and may not be applicable to longer timescales. Additionally, the observed time series are noncontinuous and this constitutes an addi-

tional uncertainty when comparing to anomalies from the remaining data sets. To test the effect of temporal coverage, the tropical ocean anomalies from the NCEP data set were recalculated using the limited temporal coverage of the observations (not shown). The T_s , CWV and SNLc time series were unaffected by the constraint. However, reductions in the anomalies by 0.15 W m^{-2} for OLRc and 0.45 W m^{-2} for Q_{LWc} are significant compared to the range of interannual variability (of order 5%). Further analysis is required to explore this uncertainty.

[67] 5. The observed relationships between variables are confined to the oceans and caution is required in extrapolating these results over nonoceanic regions.

[68] 6. The influence of aerosol on the shortwave and longwave radiation balance also influence the changes in atmospheric cooling rates. These effects have not been considered in the present study.

[69] 7. Determining net radiative cooling at the surface from satellite is problematic. The present analysis used a well calibrated record of CWV to estimate SNLc variability. While it is clear that SNLc variability is dominated by changes in CWV, the empirical estimate ignores the effects of changes in aerosol and trace gases (e.g., section 4) which contribute to changes in atmospheric emissivity. Indeed, recent observations over Europe suggest a detectable influence of trace gas changes on the surface longwave radiation budget [*Philipona et al.*, 2005]. Additionally, if systematic changes in near-surface temperature and water vapor structure arise over the period this may also influence the SNLc and Q_{LWc} variability. Therefore the empirical estimate is only representing the water vapor-related changes in SNLc. Further work is required to improve observationally based estimates of surface downward longwave radiation. This will require the use of ground-based instrumental data that is crucial in formulating and evaluating the empirical estimates of the global surface radiation budget [e.g., *Wild et al.*, 2001; *Philipona et al.*, 2005].

6. Summary

[70] Estimates of clear-sky longwave radiative cooling of the atmosphere (Q_{LWc}) are taken from reanalyses and observationally based data sets. Significant differences in the climatologies and variability are identified. A global mean Q_{LWc} of 183.5 W m^{-2} is calculated for the ERA40 climatology which, it is argued, provides the most realistic spatial climatology over the ocean. However, the quality of the clear-sky fluxes and water vapor over land regions has yet to be fully established. Interannual variations in ERA40 are affected by spurious changes in water vapor, in particular over the tropical ocean subsidence regions during 1979–1980 and for the entire tropics during the period 1985–1986. Anomalous variation in ERA40 compared to the other data sets are often characterized by anomalies in surface and top of atmosphere clear-sky radiation of opposite sign, symptomatic of errors in column mean relative humidity. It is suggested that errors in relative humidity if applying to the entire troposphere will only affect marginally the accuracy of Q_{LWc} .

[71] Interannual anomalies in surface net longwave radiation from NCEP agree well with an empirical formula based on well-calibrated satellite microwave observations of

CWV, despite the differing approaches used, although the empirical estimate produces a stronger dependence on T_s over the ascending portion of the tropical oceans. The large observed increases in CWV with surface temperature (T_s) over the tropical oceans of $3 \text{ kg m}^{-2} \text{ K}^{-1}$ are crucial in explaining a robust, positive relationship between Q_{LWc} and T_s , in particular for regions of mean ascent. For ERA40 and NCEP, both changes in SNLc and OLRc are important in explaining this relationship with cooling to the surface dominating in ascending regions and cooling to space dominating over descending branches of the tropical circulation.

[72] There is good agreement between data sets when considering the variability in Q_{LWc} , in particular during ENSO events. Over the descending portion of the tropical oceans, the calculated sensitivity dQ_{LWc}/dT_s ranges from 3.6 to $4.6 \pm 0.4 \text{ W m}^{-2} \text{ K}^{-1}$ depending on data set and time period chosen. This relationship results from increases in radiative cooling both to the surface and to space for the descending regimes, although the relative importance of the surface and top of atmosphere contribution varies between data sets and issues remain relating to satellite calibration and the prescription of greenhouse gases and aerosols which are likely to affect the accuracy of this diagnosed relationship. The range is broadly consistent with idealized sensitivity tests with a radiative transfer model in which tropospheric warming is applied for constant relative humidity. This implies that an increase in tropical mean precipitation rate, of order 0.07 to $0.1 \text{ mm day}^{-1} \text{ K}^{-1}$ is required to balance the increased radiative cooling. Further work is required to establish relationships, if any, between the clear-sky and all-sky radiative cooling and precipitation rate in the present climate on interannual and decadal to longer timescales.

[73] **Acknowledgments.** This work was funded by a NERC Advanced Fellowship (NE/C51785X/1). IDL software, licensed from the Met Office, was kindly provided by Jonathan Gregory. Thanks to Tony Slingo and Graeme Stephens for stimulating discussion. The ERA40 data were retrieved from the ECMWF data services; the NCEP data were downloaded from the NOAA-CIRES Climate Diagnostics Center; the SMMR data were extracted from the Jet Propulsion Laboratory DAAC; the SRB, ERBS and CERES data were retrieved from the NASA Langley DAAC; the SSM/I data were retrieved from <http://www.ssmi.com>; the ScaRaB data were provided by the Centre Spatial de Toulouse; the da Silva climatologies were acquired from the International research Institute from Climate and Society LDEO Climate Data Library; and the HadISST data were kindly supplied by Nick Rayner. Thanks to two anonymous reviewers for helping to improve the final manuscript.

References

Allan, R. P., and M. A. Ringer (2003), Inconsistencies between satellite estimates of longwave cloud forcing and dynamical fields from reanalyses, *Geophys. Res. Lett.*, *30*(9), 1491, doi:10.1029/2003GL017019.

Allan, R. P., V. Ramaswamy, and A. Slingo (2002), A diagnostic analysis of atmospheric moisture and clear-sky radiative feedback in the Hadley Centre and Geophysical Fluid Dynamics Laboratory (GFDL) climate models, *J. Geophys. Res.*, *107*(D17), 4329, doi:10.1029/2001JD001131.

Allan, R. P., M. A. Ringer, and A. Slingo (2003), Evaluation of moisture in the Hadley Centre climate model using simulations of HIRS water-vapour channel radiances, *Q. J. R. Meteorol. Soc.*, *129*, 3371–3389.

Allan, R. P., M. A. Ringer, J. A. Pamment, and A. Slingo (2004), Simulation of the Earth's radiation budget by the European Centre for Medium-Range Weather Forecasts 40-year reanalysis (ERA40), *J. Geophys. Res.*, *109*, D18107, doi:10.1029/2004JD004816.

Allen, M. R., and W. J. Ingram (2002), Constraints on future changes in climate and the hydrologic cycle, *Nature*, *419*, 224–232.

Bloom, S. A., et al. (2005), Documentation and validation of the Goddard Earth Observing System (GOES) data assimilation system-version 4, *Tech. Rep. NASA/TM-2005-104606*, Goddard Space Flight Cent., Greenbelt, MD.

Bosilovich, M. G., S. D. Schubert, and G. K. Walker (2005), Global changes of the water cycle intensity, *J. Clim.*, *18*, 1591–1608.

Cess, R. D. (1975), Global climate change: An investigation of atmospheric feedback mechanisms, *Tellus*, *27*, 193–198.

Ch eruy, F., and F. Chevallier (2000), Regional and seasonal variation of the clear-sky atmospheric longwave cooling over tropical oceans, *J. Clim.*, *13*, 2863–2875.

da Silva, A., A. C. Young, and S. Levitus (1994), Atlas of surface marine data 1994, vol. 1, Algorithms and procedures, *Tech. Rep. 6*, Natl. Environ. Sat. Data and Inf. Serv., U.S. Dep. of Comm., Washington, D. C.

Edwards, J. M., and A. Slingo (1996), Studies with a flexible new radiation code: I: Choosing a configuration for a large scale model, *Q. J. R. Meteorol. Soc.*, *122*, 689–719.

Gupta, S. K. (1989), A parameterization for longwave surface radiation from Sun-synchronous satellite data, *J. Clim.*, *2*, 305–320.

Harries, J. E. (1997), Atmospheric radiation and atmospheric humidity, *Q. J. R. Meteorol. Soc.*, *123*, 2173–2186.

Hartmann, D. L., and K. Larson (2002), An important constraint on tropical cloud-climate feedback, *Geophys. Res. Lett.*, *29*(20), 1951, doi:10.1029/2002GL015835.

Kalnay, E., et al. (1996), The NCEP/NCAR 40-year reanalysis project, *Bull. Am. Meteorol. Soc.*, *77*, 437–471.

Kiehl, J. T., and K. E. Trenberth (1997), Earth's annual global mean energy budget, *Bull. Am. Meteorol. Soc.*, *78*, 197–207.

Kilsby, C. G., D. P. Edwards, R. W. Saunders, and J. S. Foot (1992), Water-vapour continuum absorption in the tropics: Aircraft measurements and model comparisons, *Q. J. R. Meteorol. Soc.*, *118*, 715–748.

Lubin, D. (1994), The role of the tropical super greenhouse effect in heating the ocean surface, *Science*, *265*, 224–227.

Manabe, S., and R. T. Wetherald (1967), Thermal equilibrium of the atmosphere with a given distribution of relative humidity, *J. Atmos. Sci.*, *24*, 241–259.

McClatchey, R. A., R. A. Fenn, R. A. Selby, P. E. Voltz, and J. S. Garing (1972), Environmental research paper, *Tech. Rep. 411*, Air Force Cambridge Res. Lab., Mass.

Mitchell, J., C. A. Wilson, and W. M. Cunningham (1987), On CO₂ climate sensitivity and model dependence of results, *Q. J. R. Meteorol. Soc.*, *113*, 293–322.

Norris, J. R. (2005), Multidecadal changes in near-global cloud cover and estimated cloud cover radiative forcing, *J. Clim.*, *110*, D08206, doi:10.1029/2004JD005600.

Pavlaklis, K., D. Hatzidimitriou, C. Matsoukas, E. Drakakis, N. Hatzianastassiou, and I. Vardavas (2004), Ten-year distribution of downwelling longwave radiation, *Atmos. Chem. Phys.*, *4*, 127–142.

Philippou, R., B. D urr, A. Ohmura, and C. Ruckstuhl (2005), Anthropogenic greenhouse forcing and strong water vapor feedback increase temperature in Europe, *Geophys. Res. Lett.*, *32*, L19809, doi:10.1029/2005GL023624.

Prata, A. J. (1996), A new longwave formula for estimating downwelling clear sky radiation at the surface, *Q. J. R. Meteorol. Soc.*, *122*, 1127–1151.

Prinn, R. G., et al. (2000), A history of chemically and radiatively important gases in air deduced from ALE/GAGE/AGAGE, *J. Geophys. Res.*, *115*, 17,751–17,792.

Ramanathan, V. (1981), The role of ocean-atmosphere interactions in the CO₂ climate problem, *J. Atmos. Sci.*, *38*, 918–930.

Rayner, N. A., D. E. Parker, E. B. Horton, C. K. Folland, L. V. Alexander, D. P. Rowell, E. C. Kent, and A. Kaplan (2003), Global analyses of sea surface temperature, sea ice, and night marine air temperature since the late nineteenth century, *J. Geophys. Res.*, *108*(D14), 4407, doi:10.1029/2002JD002670.

Ringer, M. A., and R. P. Allan (2004), Evaluating climate model simulations of tropical cloud, *Tellus, Ser. A*, *56*, 308–327.

Slingo, A., J. A. Pamment, R. P. Allan, and P. Wilson (2000), Water vapour feedbacks in the ECMWF re-analyses and Hadley Centre climate model, *J. Clim.*, *13*, 3080–3098.

Soden, B. J. (2000), The sensitivity of the tropical hydrological cycle to ENSO, *J. Clim.*, *13*, 538–549.

Soden, B. J., D. L. Jackson, V. Ramaswamy, M. D. Schwarzkopf, and X. Huang (2005), The radiative signature of upper tropospheric moistening, *Science*, *310*, 841–844.

Sohn, B. (1999), Cloud-induced infrared radiative heating and its implications for large-scale tropical circulations, *J. Atmos. Sci.*, *56*, 2657–2672.

Spencer, R. W., and W. D. Braswell (1997), How dry is the tropical free troposphere? Implications for global warming theory, *Bull. Am. Meteorol. Soc.*, *78*, 1097–1106.

- Stackhouse, P. W. J., S. J. Cox, S. K. Gupta, R. C. Dipasquale, and D. E. Brown (1999), The WCRP/GEWEX Surface Radiation Budget Project Release 2: First results at 1 degree resolution, paper presented at 10th Conference on Atmospheric Radiation, Am. Meteorol. Soc., Madison, Wis.
- Stephens, G. L., A. Slingo, M. J. Webb, P. J. Minnett, P. H. Daum, L. Kleinman, I. Wittmeyer, and D. A. Randall (1994), Observations of the Earth's radiation budget in relation to atmospheric hydrology: 4. Atmospheric column radiative cooling over the world's oceans, *J. Geophys. Res.*, *99*, 18,585–18,604.
- Trenberth, K. E. (2002), Changes in tropical clouds and radiation, *Science*, *296*, 2095, doi:10.1126/science.296.5576.2095a.
- Trenberth, K. E., A. Dai, R. M. Rasmussen, and D. B. Parsons (2003), The changing character of precipitation, *Bull. Am. Meteorol. Soc.*, *84*, 1205–1217.
- Trenberth, K. E., J. Fasullo, and L. Smith (2005), Trends and variability in column-integrated atmospheric water vapor, *Clim. Dyn.*, *24*, 741–758.
- Uppala, S. M., et al. (2005), The ERA-40 re-analysis, *Q. J. R. Meteorol. Soc.*, *131*, 2961–3012.
- Wentz, F. J. (1997), A well-calibrated ocean algorithm for SMM/I, *J. Geophys. Res.*, *102*, 8703–8718.
- Wentz, F. J., and E. A. Francis (1992), Nimbus-7 SMMR ocean products, 1979–1984, *Remote Sens. Syst. Tech. Rep. 033192*, 36 pp., Santa Rosa, Calif.
- Wentz, F. J., and M. Schabel (2000), Precise climate monitoring using complementary satellite data sets, *Nature*, *403*, 414–416.
- Wielicki, B. A., et al. (2002), Evidence for large decadal variability in the tropical mean radiative energy budget, *Science*, *295*, 841–844.
- Wild, M., A. Ohmura, H. Gilgen, and A. Slingo (2001), Evaluation of downward longwave radiation in general circulation models, *J. Clim.*, *14*, 3227–3239.
- Wylie, D., D. L. Jackson, W. P. Menzel, and J. J. Bates (2005), Trends in global cloud cover in two decades of HIRS observations, *J. Clim.*, *18*, 3021–3031.
- Yang, H., and K. K. Tung (1998), Water vapor, surface temperature, and the greenhouse effect—A statistical analysis of tropical-mean data, *J. Clim.*, *11*, 2686–2697.
- Zhang, Y., W. B. Rossow, A. A. Lacis, V. Oinas, and M. I. Mishchenko (2004), Calculation of radiative fluxes from the surface to top of atmosphere based on ISCCP and other global data sets: Refinements of the radiative transfer model and the input data, *J. Geophys. Res.*, *109*, D19105, doi:10.1029/2003JD004457.

R. P. Allan, Environmental Systems Science Centre, University of Reading, Harry Pitt Building, Earley Gate, Whiteknights, P.O. Box 238, Reading RG6 6AL, UK. (rpa@mail.nerc-essc.ac.uk)